

Non-equilibrium dynamics of bosons with dipole symmetry: Large- N Keldysh approach

Md Mursalin Islam,^{1,*} K. Sengupta,² and Rajdeep Sensarma¹

¹*Department of Theoretical Physics, Tata Institute of Fundamental Research, Mumbai 400005, India.*

²*School of Physical Sciences, Indian Association for the Cultivation of Science, Kolkata 700032, India.*

(Dated: December 27, 2023)

We study the quench and the ramp dynamics of interacting N -component charged bosons with dipole symmetry using Schwinger-Keldysh field theory in the large- N limit. The equilibrium phase diagram of these bosons shows two phases in the large- N limit. The first is a normal phase where both the global $U(N)$ and the dipole symmetries are conserved and the second is a delocalized condensed phase where both the symmetries are broken. In contrast, our explicit computation of the steady state after an instantaneous quantum quench from the condensed phase shows that an additional, novel, delocalized normal phase, where the global $U(N)$ symmetry is conserved but the dipole symmetry is broken, can exist for a range of quench parameters. A study of ramp dynamics of the model shows that the above-mentioned steady state exists only above a critical ramp rate which we estimate.

I. INTRODUCTION

The behaviour of systems with symmetries that lead to conservation of multipole moments of charges (e.g. dipole moment) has recently become a question of paramount interest in the study of quantum many-body systems^{1–11}. These symmetries which implement, for example, dipole conservation are intermediate between global and gauge symmetries. It is well-known that field theories with this kind of symmetries often show a strong “UV-IR” mixing (i.e. low energy properties like ground state degeneracy are sensitive to high energy regularization of the theory)^{12–17}. These systems are also the starting point for describing matter coupled to tensorial gauge fields^{1,5,18}, which has found applications in understanding fractonic phases of matter. Such fractonic phases are characterized by low-energy excitations which are localized and can move only by creating additional excitations. In some cases, the excitations are localized in certain directions, while they are free to move in other directions. Their motion can thus be restricted along a line or a plane in three dimensional (3D) system^{18–23}.

It is generally believed that the phase diagram of interacting quantum matter out of thermal equilibrium can show a wider variety of phases than systems are in thermal equilibrium. These “phases” can be true steady states in driven dissipative systems, where the energy balance between the drive and the dissipation determines the long time behaviour^{24–29}. In fact there are protocols that engineer the bath and the drive^{30–34} to guide quantum systems into non-thermal states. An extreme example is the formation of the so-called η -paired state of the Hubbard model in non-equilibrium dynamics^{35,36}. This state is a maximum of the free energy and does not occur in thermal phases of the Hubbard model³⁷. Moreover, steady states in closed quantum systems which violate eigenstate thermalization hypothesis (ETH)^{38–42} are known to be athermal; such states occur in integrable systems^{43–45} or many-body localized systems^{46–52} and carry the imprint of the initial conditions. They can show widely different behaviour from thermal states. Similarly, in periodically driven systems the “phase” represented by such steady states occur in a prethermal regime^{53–56}. Such prethermal states can persist for a long, experi-

mentally relevant timescale, and may show several interesting features^{57–63}. These prethermal states can also show very different characteristics than the corresponding thermal states.

An important question that can be asked is the following: How can one produce a phase (either as a steady state or as a pre-thermal state), which has different symmetry content than the thermal phases of the system? Is this possible through a simple quench or a ramp of a parameter of the Hamiltonian, or does one necessarily need a more fine-tuned protocol for it? In this work, we show (using a Keldysh formalism^{64,65} and in the large- N limit) that interacting charged bosons with a dipole symmetry (that conserves dipole moment), represented by a N -component scalar field, can produce a steady state after an instantaneous quantum quench which has different symmetries from its equilibrium phases. In equilibrium, the system is either localized or Bose condensed, while the non-equilibrium steady state can support a non-condensed but dispersive phase with broken dipole symmetry for certain range of quench parameters. If the parameters are changed with a rate, this new dynamic phase disappears below a critical ramp-rate, thus reproducing the equilibrium phase diagram as one approaches the adiabatic limit.

To study this phenomenon, we consider a field theoretic model of N flavours of complex bosons in three spatial dimensions with dipole symmetry first proposed by Pretko¹. Here the bosons do not have a microscopic kinetic energy and have strongly momentum-dependent interactions; these features are consistent with global $U(N)$ charge and the corresponding dipole moment conservation. Regularizing the theory on a hyper-cubic lattice, we study its equilibrium and non-equilibrium phase diagram in the large- N limit. In equilibrium, the standard $U(N)$ model, which does not have dipole conservation, has a continuous quantum phase transition in 3D as a function of the mass and the repulsive coupling in the theory. A key question then comes up: if one enhances the symmetries to include dipole conservation, what happens to this phase diagram? The dipole conservation implies an absence of bare kinetic energy term in the model; this leads to a very different equilibrium phase diagram at zero temperature in the large- N limit. At large values of mass, the system is in a normal phase where both the $U(N)$ charge and the dipole moment is conserved. The particles in this phase are com-

pletely localized in space. As the mass is reduced the system undergoes a phase transition to a condensed phase where the $U(N)$ symmetry gets broken down to $U(N - 1)$. The dipole symmetry is also broken in this phase leading to gapless delocalized excitations with finite dispersion. These two phases are separated by a direct first-order transition. The possible phase where $U(N)$ is conserved, but dipole symmetry is broken, does not show up in the equilibrium phase diagram. We have also considered the phase diagram at a finite temperature and it is qualitatively similar to the ground state. Note that this phase diagram is qualitatively different from the phase diagram obtained in Ref. 2 for Schrödinger bosons with dipole conservation.

Interestingly, we find that the dynamical phase diagram of this system, studied within a large- N Keldysh formalism⁶⁴⁻⁶⁷, has a qualitatively different structure than its equilibrium counterpart. We follow the fate of the system starting from the ground state deep in the condensed phase, after an instantaneous quantum quench of the bare mass using a formalism developed in Ref. 65. At long times, the system goes into a quasi-stationary state, with observables oscillating around an average value. One can get an effective static description if one coarse grains the description on the scale of the time period of these oscillations. As a function of the final bare mass after the quench, we find three distinct steady states: (i) If the quench is deep into the condensed phase, the steady state has a finite condensate and breaks both $U(N)$ and dipole symmetry. (ii) As the final bare mass is increased, the condensate in the steady state continuously goes to zero at a critical value of the quenched mass. Beyond this point the system shows a gapped spectrum, with the gap increasing from zero continuously as a function of the quenched mass. In this phase, the dipole symmetry remains broken and the spectrum is dispersive, i.e. we get a steady state where the dipole symmetry is broken but $U(N)$ symmetry is restored. This phase, which has no equilibrium analogue, shows up as a steady state following a quench and is separated from the condensed phase by a second order dynamic transition. (iii) As the quenched mass is increased further, the gap shows a sharp jump at a second critical value of the quenched mass, where the curvature of the dispersion jumps from a finite value to zero. Thus, the system undergoes a first-order transition to a state where dipole symmetry is restored and the excitations are all localized. This indicates that the single first-order transition of the equilibrium state splits into a second order transition related to breaking of $U(N)$ symmetry and a separate first-order transition related to breaking of dipole symmetry.

We characterize the oscillations in the quasi-stationary state at long times. We find that the oscillation frequency scales with the gap while the amplitude increases with the decreasing value of the curvature of the dispersion. We explain this in terms of the dynamical equations. Given the system always has oscillation in the dynamics, we look at the lowest values

of the parameters to determine the transition.

We show that the presence of the phase with conserved $U(N)$ but broken dipole symmetry depends on the initial state from which the quench taken place. It vanishes when the initial state is not deep in the condensed phase, i.e. beyond a critical value of the initial mass. Beyond this value of the initial mass, the system undergoes a first-order transition similar to that found in equilibrium. This indicates that the presence of the intermediate phase depends on energy pumped into the system by the quench. This energy, pumped into the system, can be tuned by using a ramp protocol which changes the mass at a controlled rate allowing one to interpolate between the quench and the adiabatic limits. We find that the dipole broken $U(N)$ conserved phase vanishes below a critical ramp rate. For ramps slower than this critical rate, the system once again shows a single first-order transition where both $U(N)$ and dipole symmetry is broken simultaneously. We note that while the presence of the new dynamic phase depends on the energy dumped into the system, one cannot simply explain this phase in terms of thermalization at a finite energy density, since this phase does not occur in the thermal phase diagram of the system. The novel steady state is a new athermal dynamic phase of the system. We have also checked the case of the reverse quench, where we start from the state with conserved $U(N)$ and dipole symmetry. In this case, the system always shows a single first-order transition where both the symmetries are broken simultaneously.

The organization of rest of the paper is as follows. In Sec. II, we introduce the boson model and discuss its equilibrium phase diagram in the large- N limit both at zero and finite temperature. This is followed by Sec. III where we study non-equilibrium dynamics of the model for both quench and ramp protocols. Finally, we discuss our main results and conclude in Sec. IV.

II. EQUILIBRIUM PHASES OF BOSONS WITH DIPOLE SYMMETRY

In this section, we first introduce the model that we work with in Sec. II A and chart out its equilibrium properties using a large- N approach. The corresponding large- N solution is presented in Sec. II B. The zero temperature phase diagrams of the model based on the large- N solution is discussed in Sec. II C.

A. Model

We consider a system of charged bosons in 3D, whose long-wavelength low-energy thermal equilibrium properties at a temperature T are described by the Euclidean action

$$S_E = \int d^3x \int_0^\beta d\tau \left[\phi^*(x, \tau) (-\partial_\tau^2 + m_0^2) \phi(x, \tau) + \lambda_4 |\phi(x, \tau)|^4 + \lambda \left\{ (\phi^*(x, \tau))^2 \left(\phi(x, \tau) \nabla^2 \phi(x, \tau) - \vec{\nabla} \phi(x, \tau) \cdot \vec{\nabla} \phi(x, \tau) \right) + \text{h.c.} \right\} \right], \quad (1)$$

where $\beta = 1/(k_B T)$ and k_B is the Boltzmann constant which shall be set to unity for the rest of this work. This action, first proposed in Ref. 1, is invariant under: (i) a global $U(1)$ transformation $\phi(x, \tau) \rightarrow e^{i\alpha} \phi(x, \tau)$, which leads to conservation of charge $\rho = \int d^3x \rho(x)$ where

$$\rho(x) = \int d^3x \left(\partial_\tau \phi^*(x, \tau) \phi(x, \tau) - \phi^*(x, \tau) \partial_\tau \phi(x, \tau) \right), \quad (2)$$

and (ii) a dipole transformation $\phi(x, \tau) \rightarrow e^{i\vec{\gamma} \cdot \vec{x}} \phi(x, \tau)$, which leads to the conservation of the dipole moment

$$\vec{d} = \int d^3x \vec{x} \rho(x). \quad (3)$$

Note that while the $U(1)$ transformation implements a global symmetry, the dipole transformation has a status intermediate between global and gauge symmetries. This is equivalent to model A in Ref. 2.

The action Eq. 1 differs from usual interacting complex scalar theories in the following ways: (i) there are no spatial gradient terms in the quadratic part, i.e. there is no microscopic single particle kinetic energy in the system. There is however a bare mass m_0^2 which gives the gap in the single-particle spectrum when interaction strengths are set to zero. (ii) The presence of interaction terms ($\sim \lambda$) which couple to gradients of the fields and their powers. In addition, the

system has a usual ϕ^4 type local interaction with a coupling strength λ_4 . The field theory with the dipole symmetry can in principle have three different phases (a) where both $U(1)$ and dipole symmetry is maintained (b) where dipole symmetry is broken but $U(1)$ symmetry is present and (c) where both dipole and $U(1)$ symmetries are broken with the presence of a condensate. Note that one cannot have a phase with broken $U(1)$ symmetry, where the dipole symmetry is intact. The presence of the Goldstone modes would ensure that the dipole symmetry is also broken in this case.

The standard complex scalar field theory in 3D has a quantum phase transition as a function of the bare mass m_0^2 from a normal phase to a $U(1)$ symmetry broken state with a condensate characterized by $\langle \phi(x, \tau) \rangle = \sigma$. This naturally leads to the question on the nature of quantum phase transitions, if any, for a scalar field theory with dipole symmetry. We note that Ref. 2 has investigated this question for a theory with a single time derivative (the Schrödinger theory) and found that the dipole symmetry is always broken in the mean field approximation, while the system has a standard phase transition where the $U(1)$ symmetry is broken. We will see that the theory with quadratic time derivative exhibit a qualitatively different phase diagram¹.

In order to make analytic progress, we expand the ambit of the problem to a field theory with N flavours of charged bosons

$$S_E = \int d^3x \int_0^\beta d\tau \left[\sum_a \phi_a^*(x, \tau) (-\partial_\tau^2 + m_0^2) \phi_a(x, \tau) + \frac{\lambda_4}{N} \left(\sum_a |\phi_a(x, \tau)|^2 \right)^2 + \frac{\lambda}{N} \sum_{ab} \left\{ \phi_a^*(x, \tau) \phi_b^*(x, \tau) \left(\frac{1}{2} [\phi_a(x, \tau) \nabla^2 \phi_b(x, \tau) + \phi_b(x, \tau) \nabla^2 \phi_a(x, \tau)] - \vec{\nabla} \phi_a(x, \tau) \cdot \vec{\nabla} \phi_b(x, \tau) \right) + \text{h.c.} \right\} \right], \quad (4)$$

where a and b denote the flavours of the bosons. The symmetry is now enhanced to a $U(N)$ symmetry. It is useful

to Fourier transform the fields and work in the momentum-Matsubara frequency coordinates,

$$S_E = \int Dk \sum_a \phi_a^*(k) (\omega_n^2 + m_0^2) \phi_a(k) + \int \prod_{i=1}^4 Dk_i \sum_{ab} \phi_a^*(k_1) \phi_b^*(k_2) \phi_b(k_3) \phi_a(k_4) V(\{k_i\}), \quad (5)$$

where $k = (\mathbf{k}, \omega_n)$, $\omega_n = \frac{2\pi n}{\beta}$, $\int Dk = \frac{1}{\beta} \sum_n \int \frac{d^3k}{(2\pi)^3}$ and

$$V(\{k_i\}) = \left[\frac{\lambda_4}{N} + \frac{\lambda}{2N} (|\mathbf{k}_1 - \mathbf{k}_2|^2 + |\mathbf{k}_3 - \mathbf{k}_4|^2) \right] \times \delta(k_1 + k_2 - k_3 - k_4). \quad (6)$$

The continuum field theories require an ‘‘UV’’ regularization scheme for well defined answers for interacting correlators. This is usually treated within standard renormalization schemes where couplings run with cut-offs, leading to low-energy (‘‘IR’’) physical observables which are independent of the ‘‘UV’’ regularization. However, systems with dipole symmetry are known to exhibit strong ‘‘UV-IR’’ mixing, e.g. low-energy properties like degeneracy of ground states are sensitive to the ‘‘UV’’ regularization. Here we will regularize the theory on a cubic lattice of lattice spacing a with periodic boundary conditions, which amounts to replacing $|\mathbf{k}_i - \mathbf{k}_j|^2$ in Eq. 6 by

$$\epsilon(\mathbf{k}_i - \mathbf{k}_j) = \frac{4}{a^2} [\sin^2(k_i^x - k_j^x)a + \sin^2(k_i^y - k_j^y)a + \sin^2(k_i^z - k_j^z)a]. \quad (7)$$

This in turn means that we work with the regularized interaction

$$V_r(\{\mathbf{k}_i\}) = \left[\frac{\lambda_4}{N} + \frac{\lambda}{2N} (\epsilon(\mathbf{k}_1 - \mathbf{k}_2) + \epsilon(\mathbf{k}_3 - \mathbf{k}_4)) \right] \times \delta(k_1 + k_2 - k_3 - k_4) \quad (8)$$

The momenta are then restricted to the first Brillouin zone, $-\pi/a \leq k^x, k^y, k^z \leq \pi/a$. In this lattice regularized theory, we will now consider the phase diagram of the system in thermal equilibrium in the large- N limit.

B. Large- N solution

In large- N limit, bilinears of the fields, summed over flavour indices, can be assigned an average value, i.e their fluctuations are suppressed parametrically in powers of $1/N$. This mean field decoupling leads to an effective Gaussian theory, where the single particle Green’s function G is dressed by a self-energy Σ , which is determined self-consistently. The details of the large- N calculation are given in Appendix A. The single-particle Green’s function is given by

$$G(k) = \frac{1}{\omega_n^2 + \omega(\mathbf{k})^2} + |\sigma|^2 \beta \delta_{n0} (2\pi)^3 \delta^3(\mathbf{k}), \quad \text{with} \quad (9a)$$

$$\omega(\mathbf{k})^2 = m_0^2 + 2 \int Dk' G(k') NV_r(\mathbf{k}, \mathbf{k}'; \mathbf{k}, \mathbf{k}'), \quad (9b)$$

where $\sigma = \langle \phi_{a=1} \rangle / \sqrt{N}$ is the condensate fraction. For $\sigma \neq 0$, the $U(N)$ symmetry is broken down to $U(N-1)$, and Goldstone’s theorem forces the dispersion to be gapless at $\mathbf{k} = 0$. On the other hand, if the dispersion is gapped, the system must be in its normal state with $\sigma = 0$ ($U(N)$ is intact as a symmetry of the phase). This can be concisely written as a single condition, $\sigma \omega(\mathbf{k} = 0) = 0$. Putting the expression for $G(k)$ (Eq. 9a) in the equation for $\omega(\mathbf{k})$ (Eq. 9b) and perform-

ing the Matsubara sum we get the self-consistent equation,

$$\omega(\mathbf{k})^2 = m_0^2 + 2|\sigma|^2 NV_r(\mathbf{k}, 0; \mathbf{k}, 0) + 2 \int \frac{d^3k'}{(2\pi)^3} NV_r(\mathbf{k}, \mathbf{k}'; \mathbf{k}, \mathbf{k}') \frac{\coth\left(\frac{\omega(\mathbf{k}')}{2T}\right)}{2\omega(\mathbf{k}')} \quad (10)$$

Using Eq. 10, one can easily show that the dispersion can be parametrized as

$$\omega(\mathbf{k})^2 = m^2 + \kappa \epsilon(\mathbf{k}). \quad (11)$$

Putting the expressions for $NV_r(\mathbf{k}, \mathbf{k}'; \mathbf{k}, \mathbf{k}')$ and $\omega(\mathbf{k})$ in Eq. 10 we get self-consistent equations for the parameters. For the normal phase, the equations are

$$m^2 = m_0^2 + 2\lambda_4 I_1(m^2, \kappa) + 2\lambda I_2(m^2, \kappa), \quad (12a)$$

$$\kappa = 2\lambda [I_1(m^2, \kappa) - (a^2/6)I_2(m^2, \kappa)], \quad (12b)$$

and for the condensed phase, the equations are

$$\frac{\lambda_4}{\lambda} \kappa + 2[\lambda + \lambda_4(a^2/6)]I_2(0, \kappa) + m_0^2 = 0, \quad (13a)$$

$$|\sigma|^2 = \frac{\kappa}{2\lambda} - I_1(0, \kappa) + (a^2/6)I_2(0, \kappa), \quad (13b)$$

where

$$I_1(m^2, \kappa) = \int \frac{d^3k}{(2\pi)^3} \frac{\coth\left(\frac{\omega(\mathbf{k})}{2T}\right)}{2\omega(\mathbf{k})}, \quad (14a)$$

$$I_2(m^2, \kappa) = \int \frac{d^3k}{(2\pi)^3} \frac{\epsilon(\mathbf{k}) \coth\left(\frac{\omega(\mathbf{k})}{2T}\right)}{2\omega(\mathbf{k})}. \quad (14b)$$

We are now in a position to discuss the significance of the parameters m^2 , κ and σ . m^2 is the effective mass of the interacting particles, while a non-zero κ denotes the presence of an effective kinetic energy or dispersion. If $\sigma = 0$, i.e. if the $U(N)$ symmetry is not broken, m^2 is finite; in contrast, $\sigma \neq 0$ indicates the presence of a condensed phase with broken $U(N)$ symmetry ($U(N) \rightarrow U(N-1)$) and $m^2 = 0$. Moreover, if $\kappa \neq 0$, the dipole symmetry is broken, while $\kappa = 0$ denotes a system with intact dipole symmetry. For $\sigma \neq 0$, one would generically expect $\kappa \neq 0$ as the dipole symmetry is also broken in this case. Thus one can determine the symmetry of the phase simply by tracking the behaviour of σ and κ .

C. Phase Diagram at $T = 0$

We now consider the phase diagram of the system at $T = 0$ as a function of the bare mass m_0^2 . We set $a = 1$, $\coth(\omega(\mathbf{k})/2T) = 1$, and fix the couplings $\lambda = 2$ and $\lambda_4 = 2$.

Let us consider the solutions to the normal state ($\sigma = 0$) self consistent equations Eq. 12. The solutions for m^2 are plotted in Fig. 1(a). We find that solutions exist for $m_0^2 > -13.0$. The blue solid line corresponds to a solution where m^2 increases with increasing m_0^2 . This corresponds to a solution with $\kappa = 0$, i.e. both $U(N)$ and dipole symmetry are intact for this

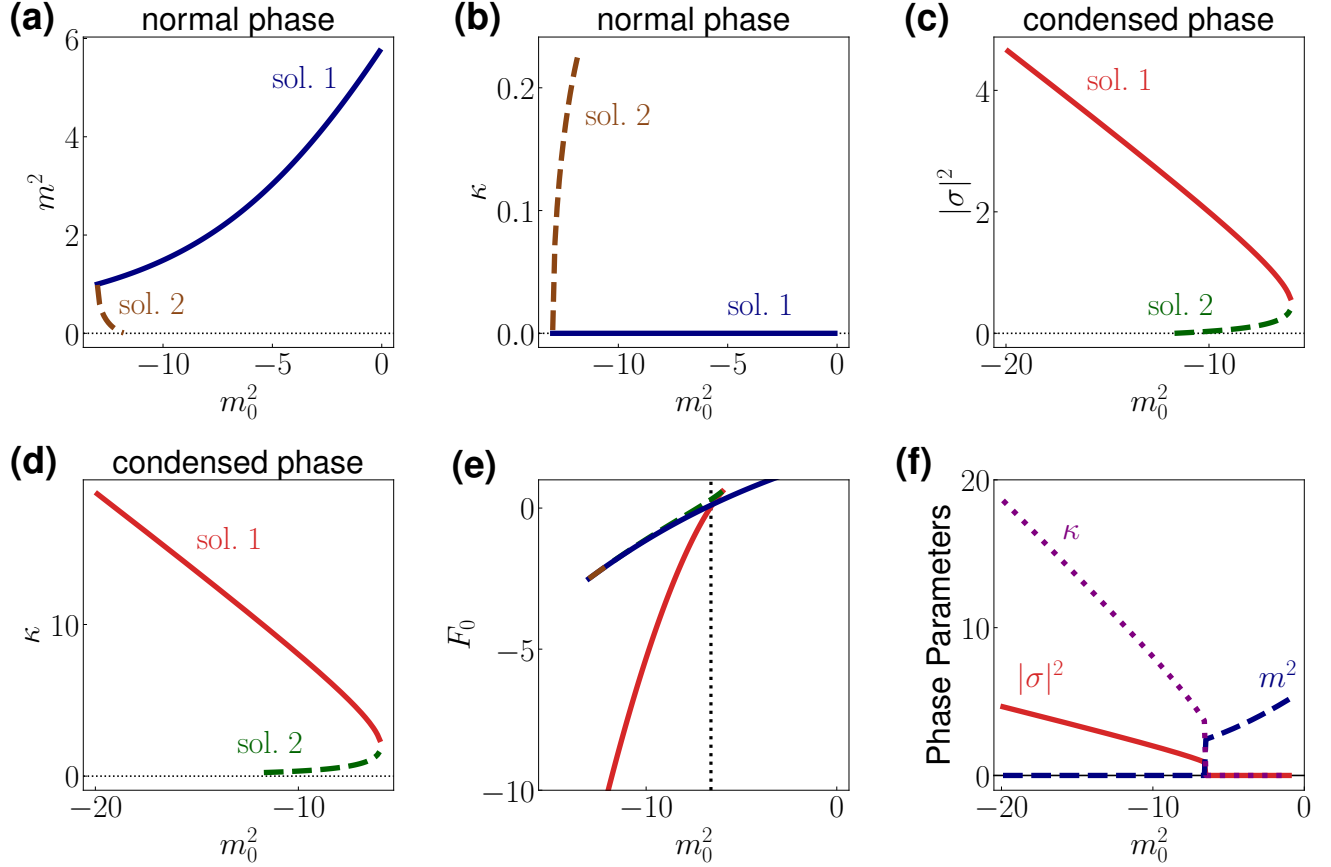


FIG. 1. Equilibrium phases of dipole conserving bosons at zero temperature. (a), (b) Solutions of the self-consistent equations for normal phase (see Eq. 12) are presented as a function of m_0^2 . One solution (shown in blue solid line) exist for $m_0^2 > -13.0$. This solution conserves both $U(N)$ and dipole symmetry. The other solution (shown in brown dashed line) exists for $-13.0 < m_0^2 < -11.8$. This solution conserves $U(N)$ but breaks dipole symmetry. (c), (d) Solutions of the self-consistent equations for condensed phase (see Eq. 13) are presented as a function of m_0^2 . One solution (shown in red solid line) exist for $m_0^2 < -6.0$. The other solution (shown in green dashed line) exists for $-11.8 < m_0^2 < -6.0$. Both the solution breaks $U(N)$ and dipole symmetry. (e) Free energy corresponding to all the solutions presented are plotted as a function of m_0^2 . The solution with the lowest free energy is the ground state. For, $m_0^2 > -6.6$ the blue solution (normal phase) is the ground state and for $m_0^2 < -6.6$ the red solution (condensed phase) is the ground state. (f) The phase parameters of the ground state as a function of m_0^2 is plotted. The blue dashed line, the purple dotted line and red solid line represent m^2 , κ and $|\sigma|^2$ respectively. For $m_0^2 > -6.6$, the ground state is a normal phase with both $U(N)$ and dipole symmetry conserved ($|\sigma|^2 = 0$, $\kappa = 0$). At $m_0^2 = -6.6$, both κ and $|\sigma|^2$ jump to finite values while m^2 goes to zero. This represents a first-order transition to the condensed phase, which simultaneously breaks both $U(N)$ and dipole symmetries. For all the plots $\lambda = \lambda_4 = 2$ and energy is measured in the units of $\sqrt[3]{\lambda_4/2a^3}$.

solution. For a small range of $-13.0 < m_0^2 < -11.8$, another solution exists, which is shown with dashed brown line. For this solution $\kappa \neq 0$ (see Fig. 1(b)), i.e. the dipole symmetry is broken although $U(N)$ is preserved. The mass m^2 decreases with increasing m_0^2 for this solution.

We now consider the solutions of the self-consistent equations (Eq. 13) in the condensed phase ($m^2 = 0$, $\sigma \neq 0$). As shown in Fig. 1(c), one solution, shown in solid red, increases with decreasing m_0^2 , and exists for $m_0^2 < -6.0$. For $-11.8 < m_0^2 < -6.0$, another solution (shown in dashed green), which decreases with decreasing m_0^2 exists. Both solutions have finite κ (Fig. 1(d)) and break both $U(N)$ and dipole symmetry.

The existence of multiple solutions to the self-consistent

equations in overlapping region of phase space indicates the occurrence of metastable states. In such a case the system is likely to undergo a first-order phase transition based on the energetics of the system. To consider this, we compute the on-shell action (free energy) of the different solutions and plot it as a function of m_0^2 in Fig. 1(e). We see that the lowest energy solution is the blue solution in the normal state for $m_0^2 > -6.6$ and the red solution in the condensed phase for $m_0^2 < -6.6$. Thus, the system transitions from a phase with both $U(N)$ and dipole symmetry to a phase where both symmetries are broken through a first-order transition. The possible normal phase with broken dipole symmetry does not show up in this phase diagram. The parameters of the lowest energy solution are plotted as a function of m_0^2 in Fig. 1(f). m^2 , κ and σ all show

a finite jump at $m_0^2 = -6.6$, which is the phase transition point.

We note that we have also calculated the phase diagram of the system for different values of λ/λ_4 . As long as both couplings are finite we qualitatively find the same phase diagram, although the location of the first-order transition points change and the jump discontinuities increase with increasing λ/λ_4 . Thus the gradient terms in the interaction drive the system towards stronger first-order transition. See Appendix B for more details.

One can also solve the self-consistent equations at finite temperature to obtain the thermal phase diagram of the system by tracking $m^2(T)$, $\sigma^2(T)$ and $\kappa(T)$ (see Appendix C for details). We find that the thermal phase diagram also consists of a fully symmetry conserved phase and a fully symmetry broken phase, separated by a direct first-order phase transition, similar to the $T = 0$ phase diagram. The critical mass for the transition shifts to the left as temperature is increased, producing the phase diagram in Fig. 2(e).

III. NON EQUILIBRIUM DYNAMICS: QUENCH AND RAMP PROTOCOLS

In this section, we consider non-equilibrium dynamics of this system of charged bosons with dipole symmetry (in the large N limit). We will be interested in the dynamics of the system after quantum quenches where parameters of the system are changed instantaneously, as well as after a ramp involving change of system parameters at a finite rate. We use a large- N Keldysh technique for this purpose which we introduce in Sec. III A. This is followed by a discussion of quench and ramp dynamics of the system starting from the condensed phase in Sec. III B and from the normal phase in Sec. III C. In Sec. III D, we explain the nature and origin of the large oscillations seen in the steady state for some values of the quench parameters.

A. Keldysh formalism

We work with the Schwinger-Keldysh formalism, where the non-equilibrium dynamics is described in terms of two fields at each space-time point^{64,66}. This formalism has been used extensively for treating non-equilibrium quantum field theory in several contexts^{52,65,67-69}, including field theories in their large- N limit⁷⁰⁻⁷⁶.

Using the standard classical and “quantum” fields, the Schwinger-Keldysh action is given by^{65,66}

$$S = \int dt \int \frac{d^3k}{(2\pi)^3} (\phi_{cl}^*(\mathbf{k}, t), \phi_q^*(\mathbf{k}, t)) \begin{pmatrix} 0 & 2[-\partial_t^2 - m_0^2(t)] \\ 2[-\partial_t^2 - m_0^2(t)] & -\Sigma^K \delta(t) \end{pmatrix} \begin{pmatrix} \phi_{cl}(\mathbf{k}, t) \\ \phi_q(\mathbf{k}, t) \end{pmatrix} + S_{int} \quad (15)$$

where

$$S_{int} = - \int dt \int \prod_{i=1}^4 \frac{d^3k_i}{(2\pi)^3} \delta(\mathbf{k}_1 + \mathbf{k}_2 - \mathbf{k}_3 - \mathbf{k}_4) V_r(\{\mathbf{k}_i\}) \quad (16)$$

$$4 [\phi_{cl}^*(\mathbf{k}_1, t) \phi_{cl}^*(\mathbf{k}_2, t) \phi_{cl}(\mathbf{k}_3, t) \phi_q(\mathbf{k}_4, t) + \phi_q^*(\mathbf{k}_1, t) \phi_q^*(\mathbf{k}_2, t) \phi_q(\mathbf{k}_3, t) \phi_{cl}(\mathbf{k}_4, t) + \text{h.c.}]$$

and we have chosen the bare mass m_0^2 to be time dependent according to a quench or a ramp protocol. The former involves a sudden change of m_0 from $(m_0)_{in}$ to $(m_0)_f$, while the latter implements a gradual ramp with a rate τ^{-1} : $m^2(t) = (m_0)_{in}^2 + ((m_0)_f^2 - (m_0)_{in}^2) f(t/\tau)$, with $f(0) = 0$ and $f(\infty) = 1$. A specific example, $f(x) = \tanh x$, shall be studied in details in this work.

In the Schwinger-Keldysh formalism, there are two independent one-particle correlators, the retarded Green’s function $G^R(\mathbf{k}, t, t') = -i\langle \phi_{cl}(\mathbf{k}, t) \phi_q^*(\mathbf{k}, t') \rangle$, which controls the evolution of the system and the Keldysh Green’s function $G^K(\mathbf{k}, t, t') = -i\langle \phi_{cl}(\mathbf{k}, t) \phi_{cl}^*(\mathbf{k}, t') \rangle$, which contains information about the time evolving one-particle distribution function in the system.

In the large- N limit, the effect of the interactions can be absorbed into a retarded self-energy (see Appendix D for details)

$$\Sigma^R(\mathbf{k}, t) = \mathbf{i} \int \frac{d^3k'}{(2\pi)^3} 4V_r(\mathbf{k}, \mathbf{k}', \mathbf{k}, \mathbf{k}') G^K(\mathbf{k}', t, t) + \frac{\mathbf{i}}{(2\pi)^3} 4V_r(\mathbf{k}, 0, \mathbf{k}, 0) G^K(0; t, t). \quad (17)$$

In this case, the retarded Green’s function can be obtained by solving

$$2[-\partial_t^2 - m^2(t) - \kappa(t)\epsilon(\mathbf{k})] G^R(\mathbf{k}, t, t') = \delta(t - t'), \quad (18)$$

where

$$m^2(t) = m_0^2(t) + 2\lambda_4|\sigma|^2(t) + 2\lambda_4 \int \frac{d^3k}{(2\pi)^3} iG^K(\mathbf{k}; t, t) + 2\lambda \int \frac{d^3k}{(2\pi)^3} \epsilon(\mathbf{k}) iG^K(\mathbf{k}; t, t) \quad (19a)$$

$$\kappa(t) = 2\lambda|\sigma|^2(t) + 2\lambda \int \frac{d^3k}{(2\pi)^3} iG^K(\mathbf{k}; t, t) - 2\lambda(a^2/6) \int \frac{d^3k}{(2\pi)^3} \epsilon(\mathbf{k}) iG^K(\mathbf{k}; t, t) \quad (19b)$$

$$|\sigma|^2(t) = \frac{1}{(2\pi)^3} iG^K(0; t, t), \quad (19c)$$

To complete the set of self-consistent equations, we need to write G^K in terms of G^R . This is done through the Dyson equation (see Appendix D and Ref. 65 for details),

$$G^K(\mathbf{k}; t, t) = [2\omega_{in}(\mathbf{k})]^2 G^K(\mathbf{k}; 0, 0) \left\{ |G^R(\mathbf{k}; t, 0)|^2 + \frac{1}{[\omega_{in}(\mathbf{k})]^2} |\bar{G}^R(\mathbf{k}; t, 0)|^2 \right\}, \quad (20)$$

where $\bar{G}^R(t, t') = \partial_{t'} G^R(t, t')$ and we have assumed that the system was initialized to Fock states corresponding to initial dispersion $\omega_{in}(\mathbf{k})$. For both the quench and the ramp dynamics $\omega_{in}(\mathbf{k})$ is the $T = 0$ equilibrium spectrum at $(m_0^2)_{in}$. Eqs. 17, 18, 19 and 20 therefore constitutes a closed set of coupled equations which provides a concrete prescription to study the non-equilibrium dynamics of this system in the large- N approximation.

B. Dynamics starting from the condensed phase

We consider the situation where the system of bosons is initialized to the interacting ground state corresponding to the couplings λ , λ_4 and $(m_0^2)_{in}$. The parameters are so chosen that the system is in the symmetry broken condensed phase with $m_{in}^2 = 0$, $|\sigma|_{in}^2 \neq 0$ and $\kappa_{in} \neq 0$. This implies that $\omega_{in}^2(\mathbf{k}) = \kappa_{in}\epsilon(\mathbf{k})$ for our problem. For most of the calculations, we will use $\lambda = \lambda_4 = 2$ and $(m_0^2)_{in} = -18.0$, unless otherwise specified.

The bare mass of the system is then instantaneously changed from $(m_0^2)_{in}$ to $(m_0^2)_f$, and the system is allowed to evolve under a closed system dynamics governed by Eqs. 17-20. The instantaneous state of the system can be characterized by $m^2(t)$ and $\kappa(t)$ which gives the instantaneous dispersion, $|\sigma|^2(t)$, which denotes the condensate density and $G^K(\mathbf{k}, t, t)$, which keeps track of the distribution function in the system. The result of such a post-quench evolution is shown in Fig. 2.

Fig. 2 (a) shows the time evolution of the parameters $m^2(t)$, $\kappa(t)$ and $|\sigma|^2(t)$, after a quench from $(m_0^2)_{in} = -18.0$ to $(m_0^2)_f = -11.5$, i.e. the final parameters also correspond to the equilibrium system in the condensed phase. In this case, it is clear that the parameters settle into a quasi-stationary state (parameters oscillate around an average value, although the amplitude of the oscillations are too small to be seen in the figure), where the average of $m^2 = 0$, while $|\sigma|^2$ and κ settle into a pattern with non-zero average values. In this case, the steady state has broken both the $U(N)$ ($U(N) \rightarrow U(N-1)$) and the dipole symmetry.

Fig. 2 (b) shows the evolution of the parameters after a

quench from $(m_0^2)_{in} = -18.0$ to $(m_0^2)_f = -10.5$. The equilibrium state at the final parameters would still correspond to a condensed phase. Once again the parameters settle down to quasi-stationary states, where $|\sigma|^2$ oscillates with very small amplitude and its lower end touches 0, while m^2 has a small but finite value, i.e. this is a normal state where the $U(N)$ symmetry is restored. However we see that the average value of κ is finite and the state thus breaks dipole symmetry. We thus recover the dipole symmetry broken normal state, which is absent in the equilibrium phase diagram, as a dynamical phase corresponding to the steady state of the system after a quantum quench.

Fig. 2(c) shows the evolution of the parameters after a quench from $(m_0^2)_{in} = -18.0$ to $(m_0^2)_f = -9.5$. The equilibrium state at the final parameters would still correspond to a condensed phase. We see that the steady (quasi-stationary) state has $|\sigma|^2 = 0$ and a finite gap m^2 . m^2 has large amplitude oscillations around the average value, but the lowest value of m^2 remains positive. The curvature κ shows large oscillations around a small value, such that the lowest value of κ reaches 0. We identify this as the phase where both dipole and $U(N)$ symmetry are restored.

We now consider the average long time value of the steady state parameters as a function of the final quenched mass $(m_0^2)_f$. This average is calculated by averaging the values of the parameters over a time range from 500 to 1000 to get rid of the effects of oscillations. Here the time is measured in the units of $\sqrt[3]{2a^3/\lambda_4}$. We have checked that changing the range of this averaging does not change the answers qualitatively, and changes them quantitatively by at most 2%.

These average values are plotted in Fig. 2(d) with the amplitude of the oscillations setting the errorbar shown in the figure. We find that for $(m_0^2)_f < -11.0$, the condensate density and the curvature is finite, while the gap is zero. At $(m_0^2)_f = -11.0$, the condensate density continuously goes to zero through a second order dynamical transition; the gap also starts becoming finite just beyond this point. Note that the curvature κ is finite and shows a smooth behaviour around this transition point. Thus, one expect this transition to be a second order transition, across which $U(N)$ symmetry is

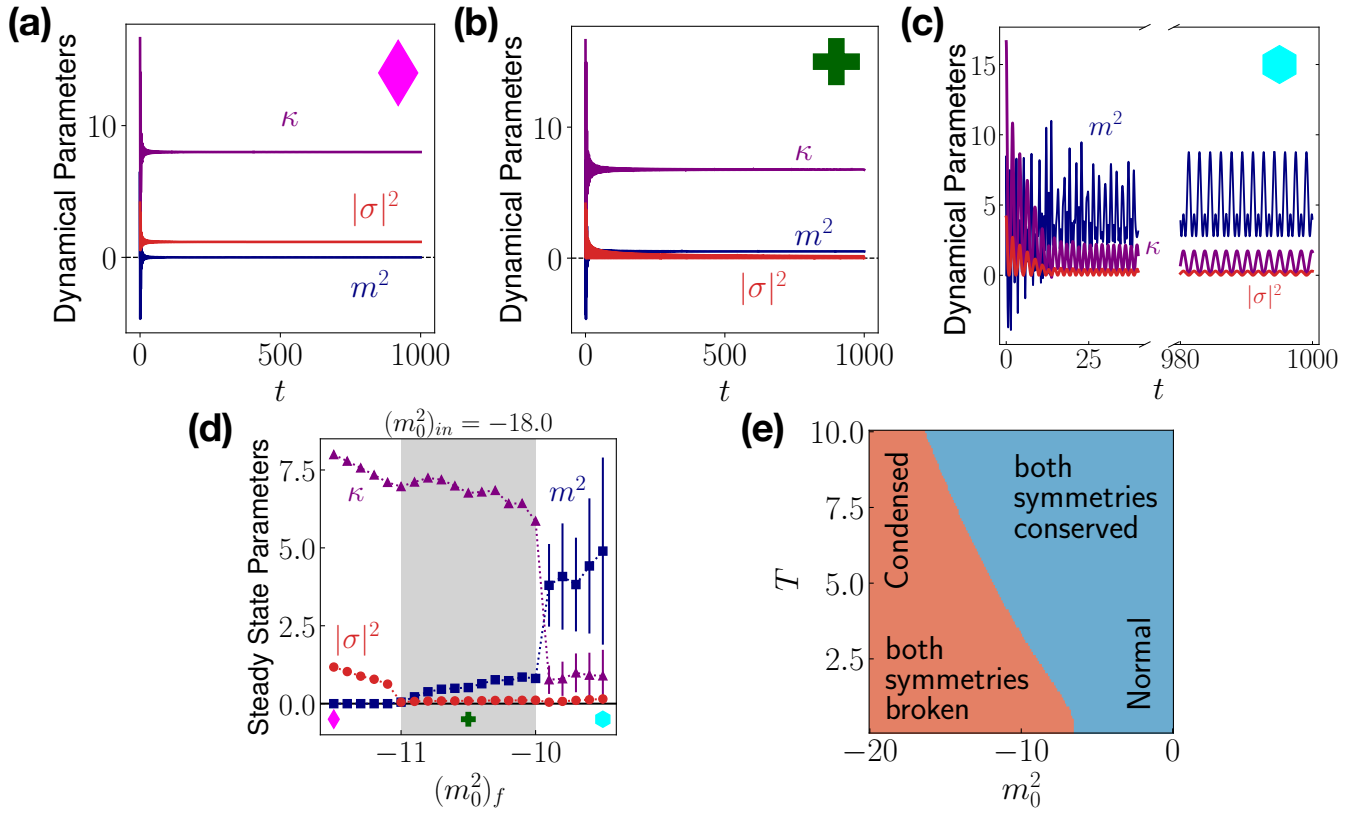


FIG. 2. Dynamics of parameters after a sudden quench of m_0^2 starting from ground state in condensed phase with $(m_0^2)_{in} = -18.0$ and $\lambda = \lambda_4 = 2$. The initial values of the parameters are $(|\sigma|^2)_{in} = 4.15$, $(\kappa)_{in} = 16.63$ and $(m^2)_{in} = 0$. $(m_0^2)_f$ denotes the final value of m_0^2 after the quench. Here the time is measured in the units of $\sqrt[3]{2a^3/\lambda_4}$. (a) Dynamics of the parameters for $(m_0^2)_f = -11.5$ is shown. At long times, $m^2 = 0$ while κ and $|\sigma|^2$ remain finite. This represents a condensed phase. (b) Dynamics of the parameters for $(m_0^2)_f = -10.5$ is shown. At long times, m^2 gains finite value while $|\sigma|^2$ shows small oscillation with its lowest value touching 0 and κ remains finite. This represents a phase where dipole symmetry is broken but $U(N)$ is restored. This is a dynamical phase which is absent at equilibrium. (c) Dynamics of the phase parameters for $(m_0^2)_f = -9.5$ is shown. The x-axis is broken to accommodate both the initial transients and steady state dynamics. At long times, m^2 fluctuates largely with a finite time-averaged value. It stays well above 0. κ and $|\sigma|^2$ fluctuates with their lowest value very close to 0. This represents a normal phase. (d) Steady state time-averaged values (averaged for $t = 500 - 1000$) of the dynamical parameters are shown as a function of $(m_0^2)_f$. The error-bars represent amplitude of the oscillations at long times. We see two transitions separating three kinds of phases. At $(m_0^2)_f = -11.0$, $|\sigma|^2$ smoothly goes to 0 (its lowest value touches 0) and m^2 attains finite value while κ remains finite. At $(m_0^2)_f = -9.9$, κ falls sharply and m^2 rises further. So, for $(m_0^2)_f < -11.0$, we have condensed phase with charge and dipole symmetry broken. For $(m_0^2)_f > -9.9$, we have the normal phase with conserved charge and dipole. Between these two transitions, charge is conserved but dipole is not. This is a dynamical phase which is absent in equilibrium. So, $U(N)$ and dipole symmetries get restored at different points unlike the case in equilibrium where this happens in a single transition. The positions of $(m_0^2)_f$ values for which the dynamics of the dynamical parameters are shown in (a), (b) and (c) are indicated by a magenta diamond, a green '+' and a cyan hexagon respectively. (e) Thermal phase diagram of bosons with dipole symmetry in the $m_0^2 - T$ plane. The light red shaded area hosts condensed phase ($m^2 = 0, \kappa > 0, |\sigma|^2 > 0$) where $U(N)$ and dipole symmetries both are broken. The light blue shaded area is for the normal phase ($m^2 > 0, \kappa = 0, |\sigma|^2 = 0$) where both the $U(N)$ and dipole symmetries are conserved. The boundary between these shaded areas indicate a first-order transition. The critical m_0^2 decreases with increasing temperature. Note that the intermediate dynamical phase with conserved $U(N)$ but broken dipole symmetry is absent in the thermal phase diagram.

broken down to $U(N - 1)$. As the final mass $(m_0)_f$ is increased, at $(m_0^2)_f = -9.9$, the curvature shows a rapid decrease while the gap jumps to a finite value; this constitutes a clear non-analytic behaviour. The fluctuations in the gap and the curvature, as measured by the oscillation amplitudes grow significantly beyond this jump (In Fig. 2(d), the error bars are smaller than the symbol size for $(m_0^2)_f < -9.9$). Note that the average curvature does not immediately go to zero, but its lowest value goes below it eventually. So, we consider the

sharp change in κ and m^2 as the indication of the transition point. We thus have a second transition where the dipole symmetry is restored. We use the point where the curvature and gap shows a jump discontinuity to define the first-order transition which restores dipole symmetry. Both these transitions occur to the left of the equilibrium transition at $m_0^2 = -6.6$. Thus the single first order transition in equilibrium is split into a continuous transition and a first-order transition in the dynamic phase diagram of the system.

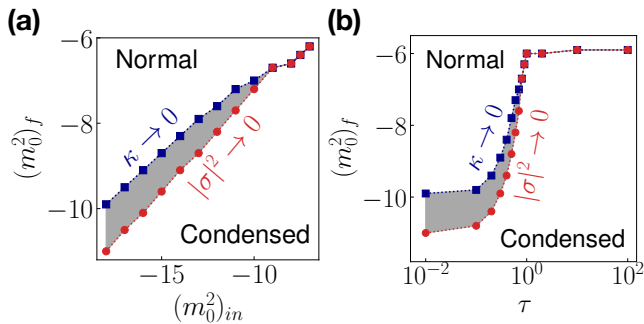


FIG. 3. Dynamical phase diagram for non-equilibrium dynamics of bosons with dipole symmetry: (a) The steady state phases after a quantum quench from $(m_0^2)_{in}$ to $(m_0^2)_f$. The normal phase has conserved $U(N)$ and dipole symmetry, while both symmetries are broken in the condensed phase. The shaded region shows the dynamical phase with $U(N)$ symmetry, where dipole conservation is broken. The phase boundaries are obtained by considering critical quench parameters where $|\sigma|^2 \rightarrow 0$ (red points) and $\kappa \rightarrow 0$ (blue points) in the steady state. Note that for $(m_0^2)_{in} > -9.0$, the system has direct first-order transition from condensed to normal phase. The intermediate phase exists for $(m_0^2)_{in} < -9.0$ and occupies larger phase-space as $(m_0^2)_{in}$ is reduced. (b) The steady state phases after a ramp of m_0^2 from $(m_0^2)_{in} = -18.0$ to $(m_0^2)_f$ with a ramp timescale τ (in the $\tau - (m_0^2)_f$ plane). In the normal (condensed) phase both $U(N)$ and dipole symmetries are present (broken), while the shaded region shows the intermediate phase, where $U(N)$ symmetry is conserved but dipole symmetry is broken. Note that the intermediate phase vanished beyond $\tau = 0.8$, and the system shows a first-order transition from condensed to normal phase beyond this value of τ (similar to the equilibrium phase diagram). Here $\lambda = \lambda_4 = 2$ for both the plots and τ is measured in the units of $\sqrt[3]{2a^3/\lambda_4}$.

Till now, we have discussed the phase diagram of the steady state after a quench from $(m_0^2)_{in} = -18.0$ to different values of $(m_0^2)_f$. However, one can ask: does the presence/size of the intermediate phase depend on the initial mass from where we are starting our quench? To see this, we first vary the initial $(m_0^2)_{in}$ and plot the critical quenched $(m_0^2)_f$ where the jump occurs and where the condensate vanishes. The two critical quench parameters (final bare mass where the transitions take place) are plotted as a function of $(m_0^2)_{in}$ in Fig. 3(a). The intermediate phase exists when these two values are different as shown by the shaded region. We see that the intermediate phase exists for $(m_0^2)_{in} < -9.0$. For $(m_0^2)_{in} > -9.0$, which is still in the condensed phase, the system directly jumps from the symmetry broken phase to the phase where both symmetries are restored. Note that while different initial quench masses lead to different amount of energy dumped in the system, this is not the sole parameter governing the phase diagram (e.g. the energy dumped at the critical final mass varies quite a lot with changes in the initial mass).

There is a different way to control the amount of energy dumped due to change in parameters of the system. Instead of an instantaneous quench, one can change m_0^2 smoothly in time through

$$m_0^2(t) = (m_0^2)_{in} + \left[(m_0^2)_f - (m_0^2)_{in} \right] \tanh(t/\tau), \quad (21)$$

where τ is the ramp timescale. $\tau \rightarrow 0$ leads to an instantaneous quench, while $\tau \rightarrow \infty$ depicts an adiabatic change of the parameter. We track the dynamics of the system undergoing this ramp at large times ($t \gg \tau$) and obtain steady average values of m^2 and κ . In Fig. 3(b), the two critical $(m_0^2)_f$ s, where σ^2 vanishes and where κ and m^2 jumps, are plotted as a function of the ramp timescale. The phase space for the intermediate dipole symmetry broken normal state (shown by the shaded region) shrinks with increasing τ and vanishes beyond a finite value of $\tau = 0.8$. The system thus undergoes a dynamical phase transition as a function of the ramp time, with the intermediate phase absent in the adiabatic limit. In the adiabatic limit, the system follows the condensed phase and directly shows a first-order transition to a normal state with conserved dipole symmetry. We thus see that the ramp rate is a crucial parameter which determines the phase diagram of the system.

Finally, we consider what is likely to happen if we treat the dynamics beyond the large- N approximation. The sub-leading terms in the action would introduce scattering between the momentum modes, effectively introducing dissipation for the one particle dynamics. In this case, the intermediate phase will disappear over a longer timescale and the system will thermalize at the longest time-scales. However since the time-scale is parametrically larger than the timescales involved in the large- N dynamics, one would expect the intermediate phase to show up as a long-lived prethermal state of the system.

C. Dynamics starting from the normal phase

It is well-known that systems undergoing first-order transitions typically show hysteresis, and so one would normally expect that the dynamics of the system starting from the condensed phase will not be the same as the dynamics of the system starting from the normal phase. We will now focus on the dynamics of this system starting from a ground state in the normal phase, which preserves both the $U(N)$ and the dipole symmetry.

We consider the dynamics of the system after a sudden quantum quench. The system is initialized in the ground state of normal phase with $(m_0^2)_{in} = -4.0$ and m_0^2 is suddenly quenched to a more negative value $(m_0^2)_f$. At the initial point, $\kappa_{in} = 0$ and $m_{in}^2 = 3.49$. To allow for the possibility that the dynamics can lead to symmetry broken steady state, we start with a tiny seed value for the condensate with $(|\sigma|^2)_{in} = 10^{-4}$. One can think of this as a seed value which may grow, shrink or remain the same under the dynamics. The system is then allowed to evolve to a steady state under its own dynamics, where the parameters oscillate around an average value. In Fig. 4(a), we show the time dependence of the parameters $|\sigma|^2(t)$, $\kappa(t)$ and $m^2(t)$ after a quench to $(m_0^2)_f = -10$. We find that κ and $|\sigma|^2$ vanishes in the steady state, while m^2 oscillates around a finite value, i.e. the steady state has $U(N)$ and dipole symmetries. In Fig. 4(b), we show the same parameters after a quench to $(m_0^2)_f = -18$. In

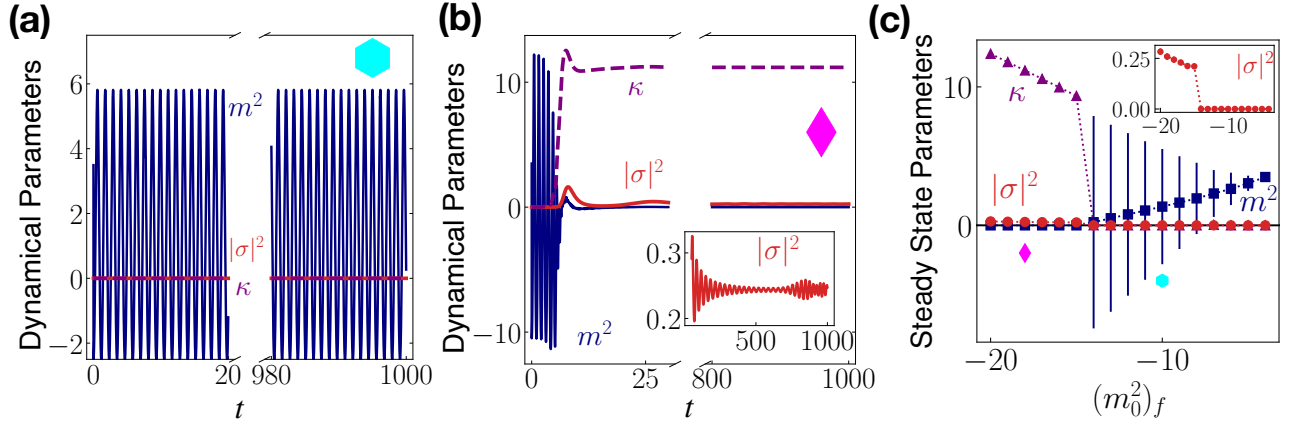


FIG. 4. Dynamics of parameters after a sudden quench of m_0^2 starting from ground state in normal phase with $(m_0^2)_{in} = -4.0$ and $\lambda = \lambda_4 = 2$. Initial values of the phase parameters are $(m^2)_{in} = 3.49$, $(\kappa)_{in} = 0.0$ and $(|\sigma|^2)_{in} = 10^{-4}$. $(m_0^2)_f$ denotes the final value of m_0^2 after the quench. The time is measured in the units of $\sqrt[3]{2a^3/\lambda_4}$. (a) Time dependence of the parameters for $(m_0^2)_f = -10.0$. m^2 oscillates around a finite value, while κ and $|\sigma|^2$ vanish. This represents a normal phase where both the symmetries are conserved. (b) Time evolution of the parameters for $(m_0^2)_f = -18.0$. At long times, m^2 goes to zero and κ and $|\sigma|^2$ (as shown in the inset) gain finite values. This indicates that the system goes to the condensed phase at long times. In (a) and (b) the x-axis is broken to accommodate both the initial transients and steady state dynamics. (c) Long time average values (averaged for $t = 500 - 1000$) of the dynamical parameters are shown as a function of $(m_0^2)_f$. The error-bars represent amplitudes of the oscillations a long times. As $(m_0^2)_f$ is decreased, m^2 drops but its fluctuation increases until $(m_0^2)_f = -14.9$ where both its average value and fluctuation go to zero. Immediately after this point, κ jumps to finite value. At the same point the condensate $|\sigma|^2$ also attains finite value, which is significantly higher than the initial seed value of 10^{-4} , as shown in the inset. This indicates a first-order transition to the condensed phase. The final masses for which dynamics of the parameters are shown in (a) and (b) are indicated by a cyan hexagon and a magenta diamond respectively in (c).

this case, the steady state has $m^2 = 0$ and finite κ . We see from the inset that the condensate fraction $|\sigma|^2$ is non-zero in this steady state. The system is thus in a state with broken $U(N)$ and dipole symmetries. In Fig. 4(c), we present the steady state average values (averaged for $t = 500 - 1000$ in the units of $\sqrt[3]{2a^3/\lambda_4}$) of the parameters as a function of $(m_0^2)_f$. The error bar represents the amplitude of oscillation around the average value. As $(m_0^2)_f$ is decreased, the gap m^2 drops but its fluctuation increases until a point where both its average value and fluctuation go to zero at $(m_0^2)_f = -14.9$. Immediately after this, the curvature κ becomes finite with very small fluctuations (not visible on the scale of the figure). At the same point, the condensate $|\sigma|^2$ also attains small finite value, as seen in the inset of Fig. 4(c). Note that this value is much larger than the seed value used, which indicates the instability towards a broken symmetry phase. Note that both κ and $|\sigma|^2$ shows a jump discontinuity at the same point, thus the steady state under the reverse dynamics from the normal phase shows a single first-order transition, where both the $U(N)$ and the dipole symmetry are broken simultaneously, similar to the equilibrium phase diagram. We have checked that changing the seed value for $|\sigma|^2$ to 10^{-6} changes the location of the transition slightly ($(m_0^2)_f$ changes from -14.9 to -15.2). However, the value of $|\sigma|^2$ in the steady state in the symmetry broken phase depends strongly on the seed value, as one would expect for an instability.

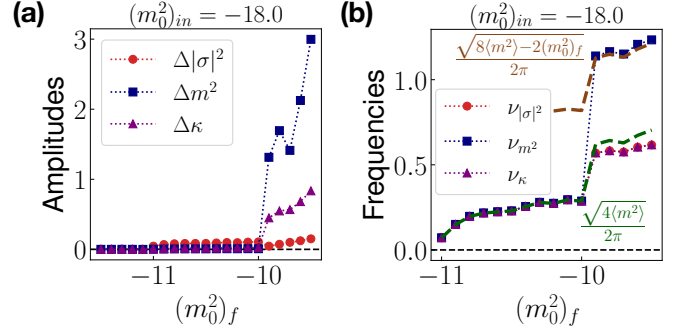


FIG. 5. Oscillations of the parameters in the steady state following a sudden quench of m_0^2 starting from the condensed phase with $(m_0^2)_{in} = -18.0$ and $\lambda = \lambda_4 = 2$. $(m_0^2)_f$ denotes the final value of m_0^2 after the quench. (a) Amplitudes of the oscillations in the steady state. The amplitudes of m^2 and κ are significantly larger for $(m_0^2)_f \geq -9.9$. The steady states correspond to the normal phase, where time-averaged m^2 is large and κ and $|\sigma|^2$ touch zero. (b) Dominant frequencies of the oscillations in the steady state. For $(m_0^2)_f \geq -9.9$, where the oscillations are more prominent, the frequencies agree well with the frequencies that one gets from the dynamical equations. ν_κ and $\nu_{|\sigma|^2}$ agree with $\sqrt{4\langle m^2 \rangle}/2\pi$ sketched by the dashed green line and ν_{m^2} agrees with $\sqrt{8\langle m^2 \rangle - 2(m_0^2)_f}/2\pi$ sketched by the dashed brown line. Here $\langle m^2 \rangle$ denotes the time-averaged m^2 in the steady state.

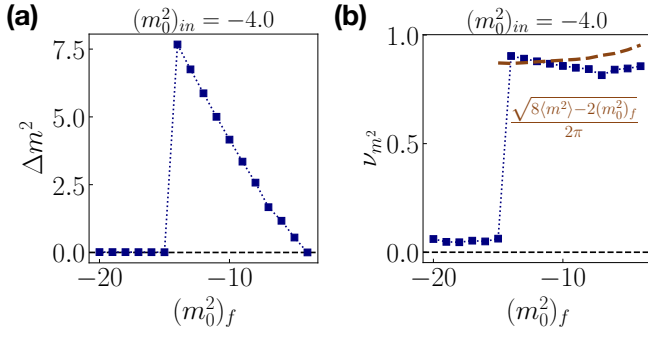


FIG. 6. Oscillations of the parameter m^2 in the steady state following a sudden quench of m_0^2 starting from the normal phase with $(m_0^2)_{in} = -4.0$ and $\lambda = \lambda_4 = 2$. $(m_0^2)_f$ denotes the final value of m_0^2 after the quench. (a) Amplitudes of the oscillations in the steady state. The amplitudes of m^2 and κ are significantly larger for $(m^2)_f > -14.9$. The steady states correspond to the normal phase, where time-averaged m^2 is finite and κ and $|\sigma|^2$ are zero. (b) Dominant frequencies of the oscillations in the steady state. For $(m_0^2)_f > -14.9$, where the oscillations are more prominent, the frequencies agree well with the frequencies that one gets from the dynamical equations. ν_{m^2} agrees with $\sqrt{8\langle m^2 \rangle - 2(m_0^2)_f}/2\pi$ sketched by the dashed brown line. Here $\langle m^2 \rangle$ denotes the time-averaged m^2 in the steady state.

D. Oscillations in the Steady State

Till now, we focused on the time-averaged values of the parameters in the steady state. However, from Figs. 2(d) and 4(c) it is clear that the parameters have large oscillations for some values of $(m_0^2)_f$, where the time-averaged κ is very small and time-averaged m^2 is finite and large. In this section, we characterize these oscillations and explain their origin.

Let us first consider the case of quench from the condensed phase. In Fig 5, the amplitudes and frequencies of the oscillations of the parameters at long times ($t = 800 - 1000$ in the units of $\sqrt[3]{2a^3/\lambda_4}$) are plotted as a function of $(m_0^2)_f$. In Fig. 5(a), the amplitudes of oscillations are very small for $(m_0^2)_f < -9.9$, and they increase significantly for $(m_0^2)_f > -9.9$. This coincides with the jump in m^2 and κ as shown in Fig. 2(d). In Fig. 5(b), the frequencies of oscillations are plotted. In the region, where the parameters oscillate with large

amplitudes, κ and $|\sigma|^2$ have the same frequency while m^2 oscillates with a different frequency. Both the amplitude and frequency show sharp jumps as the system goes from the intermediate dynamical phase to the normal phase. Similar kind of behaviour is also observed when the system is quenched from the normal phase as shown in Fig. 6. In this case only m^2 shows large oscillations for $(m_0^2)_f > -14.9$, which corresponds to the region in Fig. 4(c) where steady state value of m^2 is finite while κ and $|\sigma|^2$ are zero. The frequency of the oscillation also jumps at the same point as can be seen from Fig. 6(b). So, one can conclude that when the time-averaged value of κ is close to zero and time-averaged value of m^2 is finite, the parameters show larger and faster oscillations.

To explain these observations, one needs to look back at the dynamical equations depicted in Eqs. 18, 19 and 20. In Eq. 18, one can make a simple approximation to calculate $G^R(\mathbf{k}; t, t')$ in the steady state by considering the time averaged values of the parameters m^2 and κ , denoted by $\langle m^2 \rangle$ and $\langle \kappa \rangle$ respectively. This results in

$$G^R(\mathbf{k}; t, t') = -\Theta(t - t') \frac{\sin(\omega(\mathbf{k}))(t - t')}{2\langle \omega(\mathbf{k}) \rangle}, \quad (22)$$

where $\langle \omega(\mathbf{k}) \rangle = \sqrt{\langle m^2 \rangle + \langle \kappa \rangle \epsilon(\mathbf{k})}$. Using this and Eq. 20 one gets

$$\begin{aligned} G^K(\mathbf{k}; t, t) &= G^K(\mathbf{k}; 0; 0) \left\{ \frac{\omega_{in}(\mathbf{k})^2}{\langle \omega(\mathbf{k}) \rangle^2} \sin^2 \langle \omega(\mathbf{k}) \rangle t + \cos^2 \langle \omega(\mathbf{k}) \rangle t \right\}. \end{aligned} \quad (23)$$

Re-arranging the time-dependent parts one gets,

$$\begin{aligned} G^K(\mathbf{k}; t, t) &= \frac{\langle \omega(\mathbf{k}) \rangle^2 + \omega_{in}(\mathbf{k})^2}{4\langle \omega(\mathbf{k}) \rangle^2 \omega_{in}(\mathbf{k})} + \frac{\langle \omega(\mathbf{k}) \rangle^2 - \omega_{in}(\mathbf{k})^2}{4\langle \omega(\mathbf{k}) \rangle^2 \omega_{in}(\mathbf{k})} \cos 2\langle \omega(\mathbf{k}) \rangle t. \end{aligned} \quad (24)$$

Now, from Eq. 19, it can be noted that both $m^2(t)$ and $\kappa(t)$ involve integration of $G^K(\mathbf{k}; t, t)$ over momentum. The time-dependent parts of them involve the integrals

$$\tilde{I}_1(t) = \int d\epsilon g(\epsilon) \frac{(\langle m^2 \rangle + \langle \kappa \rangle \epsilon) - (m_{in}^2 + \kappa_{in} \epsilon)}{4(\langle m^2 \rangle + \langle \kappa \rangle \epsilon) \sqrt{m_{in}^2 + \kappa_{in} \epsilon}} \cos \left(2\sqrt{\langle m^2 \rangle + \langle \kappa \rangle \epsilon} t \right) \quad \text{and} \quad (25a)$$

$$\tilde{I}_2(t) = \int d\epsilon g(\epsilon) \frac{(\langle m^2 \rangle + \langle \kappa \rangle \epsilon) - (m_{in}^2 + \kappa_{in} \epsilon)}{4(\langle m^2 \rangle + \langle \kappa \rangle \epsilon) \sqrt{m_{in}^2 + \kappa_{in} \epsilon}} \epsilon \cos \left(2\sqrt{\langle m^2 \rangle + \langle \kappa \rangle \epsilon} t \right). \quad (25b)$$

Here, we have transformed the momentum integrations to energy integrations using the transformation $\epsilon = \epsilon(\mathbf{k})$, where $g(\epsilon)$ is the density of states of the lattice dispersion in 3D. These are the main time-dependent terms in $m^2(t)$ and $\kappa(t)$, and their behaviour determines the nature of oscillations in the parameters. Note that $\langle \kappa \rangle$ determines the bandwidth of the phase factor. So, large $\langle \kappa \rangle$ causes large dephasing i.e. summing over different phase rotations cancels each other. This results in small \tilde{I}_1 and \tilde{I}_2 and hence the parameters do not show large oscillations as long as $\langle \kappa \rangle$ stays sufficiently large. On the other hand, a small $\langle \kappa \rangle$ fails to provide enough bandwidth for the phase factors to cancel them. Another way to see this is that performing the integration

brings down factors of $\langle \kappa \rangle$ in the denominator and the integrals becomes large when $\langle \kappa \rangle$ is small. As an example let's consider \tilde{I}_1 for the case of quench from condensed phase. Considering only the leading order terms one gets

$$\tilde{I}_1(t) \sim \int d\epsilon g(\epsilon) \frac{1}{4\sqrt{\kappa_{in}\epsilon}} \cos\left(\sqrt{4\langle m^2 \rangle} + \frac{\langle \kappa \rangle}{\sqrt{\langle m^2 \rangle}} \epsilon\right) t \sim \frac{\sqrt{\langle m^2 \rangle}}{\langle \kappa \rangle} (\text{oscillating term}). \quad (26)$$

So, when $\langle \kappa \rangle$ is small the integrals \tilde{I}_1 and \tilde{I}_2 oscillate with large amplitudes and hence one can expect the parameters to have large oscillations. This explains the observed large oscillations of the parameters in the dynamical phase diagrams (see Figs. 2(d) and 4(c)) as shown in Fig. 5(a) and 6(a) where $\langle \kappa \rangle$ is small.

To understand the oscillation frequencies it is useful to take the dynamical equations for the parameters in Eq. 19 and get differential equations for the parameters out of them. Considering only the simplest terms, one gets

$$\partial_t^2 \kappa(t) \sim -2m^2(t)\kappa(t) \quad \text{and} \quad (27a)$$

$$\partial_t^2 m^2(t) \sim -2[m^2(t)]^2 + 2(m_0^2)_f m^2(t), \quad (27b)$$

respectively. So, the ‘instantaneous’ oscillation frequencies depends on $m^2(t)$. One can consider time-averaged value of it with a factor of $\sqrt{2}$ to account for the fluctuations and get the oscillation frequencies for $\kappa(t)$ and $m^2(t)$

$$\tilde{\nu}_\kappa = \sqrt{4\langle m^2 \rangle}/2\pi \quad (28a)$$

$$\tilde{\nu}_{m^2} = \sqrt{8\langle m^2 \rangle - 2(m_0^2)_f}/2\pi. \quad (28b)$$

From Figs. 5(b) and 6(b) it can be noted that these frequencies agree well with the observed frequencies in the dynamics of the parameters, when they have large oscillations.

IV. CONCLUSION

We have studied the equilibrium and non-equilibrium phase diagram of charged interacting bosons with $U(N)$ and dipole symmetries in the large- N limit. The mass m^2 , the dispersion κ and the condensate density $|\sigma|^2$ can be used to track the phases of this system. In thermal equilibrium, the system shows a first-order phase transition from a phase where both $U(N)$ and dipole symmetry are intact to a phase where both are broken. Around this transition, the system has several metastable states of different symmetries and their energetics leads to a first-order transition.

In contrast, the steady state of the system starting from an initial condensed phase and after a quantum quench of the

bare mass parameter m_0^2 from $(m_0^2)_{in}^2$ to $(m_0^2)_f^2$ shows a more interesting phase diagram. Here, for a range of $(m_0^2)_f^2$, the condensate density goes to zero in a continuous manner. This indicates a dynamical second order transition. The transition restores the $U(N)$ symmetry while breaking the dipole symmetry; this leads to a dipole symmetry broken normal phase which has no equilibrium counterpart. Upon further increase of $(m_0^2)_f^2$, the dipole symmetry broken normal phase gives way to a normal dipole symmetry restored phase through a first-order phase transition. A quench from the normal state do not see the intermediate phase; here we find a direct first-order transition from the dipole symmetry broken normal to the condensed phase similar to the equilibrium phase diagram.

Our study of the quantum ramp dynamics elucidates the role of ramp dynamics in realizing the intermediate phase. We find that the intermediate phase shrink with increasing τ and vanishes when it is above a critical τ_c ; this leads to an interpolation between the quench behaviour $\tau \rightarrow 0$ and the adiabatic behaviour $\tau \rightarrow \infty$.

To conclude, our study shows bosonic systems with dipole symmetry show interesting equilibrium and non-equilibrium phase diagrams. The presence of metastable states leads to non-trivial phenomenology under quench dynamics, where symmetry broken states, which do not exist in equilibrium, can appear as steady states for certain initial conditions. These steady states are likely to exist over a prethermal timescale; this timescale, however, is controlled by higher order $1/N$ terms in the action and is expected to be large for large- N . They will lead to a slow thermalization in these systems, a detailed study of which is left as a subject of future study.

ACKNOWLEDGMENTS

The authors are grateful to Pranay Gorantla and Leticia F. Cugliandolo for useful discussions and suggestions. MMI and RS acknowledge the use of computational facilities at the Department of Theoretical Physics, Tata Institute of Fundamental Research, Mumbai for this paper. MMI and RS acknowledge support of the Department of Atomic Energy, Government of India, under Project Identification No. RTI 4002. KS thanks DST, India for support through SERB project JCB/2021/000030.

Appendix A: Large- N saddle point equations

In this appendix we derive the saddle point equations starting from a large- N action for the dipole conserving bosons. We will follow the method described in Ref. 2. We start from the euclidean action (see Eq. 1) in d spatial dimensions

$$S_E = \int d^d x \int_0^\beta d\tau [\phi^*(x, \tau)(-\partial_\tau^2 + m_0^2)\phi(x, \tau) + \lambda_4 |\phi(x, \tau)|^4 + \lambda \left\{ (\phi^*(x, \tau))^2 \left(\phi(x, \tau) \nabla^2 \phi(x, \tau) - \vec{\nabla} \phi(x, \tau) \cdot \vec{\nabla} \phi(x, \tau) \right) + \text{h.c.} \right\}]. \quad (\text{A1})$$

We move to a field theory with N flavours of charged bosons

$$S_E = \int d^d x \int_0^\beta d\tau \left[\sum_a \phi_a^*(x, \tau)(-\partial_\tau^2 + m_0^2)\phi_a(x, \tau) + \frac{\lambda_4}{N} \left(\sum_a |\phi_a(x, \tau)|^2 \right)^2 + \frac{\lambda}{N} \sum_{ab} \left\{ \phi_a^*(x, \tau)\phi_b^*(x, \tau) \left(\frac{1}{2} [\phi_a(x, \tau)\nabla^2\phi_b(x, \tau) + \phi_b(x, \tau)\nabla^2\phi_a(x, \tau)] - \vec{\nabla}\phi_a(x, \tau) \cdot \vec{\nabla}\phi_b(x, \tau) \right) + \text{h.c.} \right\} \right], \quad (\text{A2})$$

where a, b denote the flavours of the bosons.

It is convenient to work in the momentum-Matsubara frequency space. We make the Fourier transform $\phi_a(x, \tau) = \int Dk e^{i\mathbf{k}\cdot\mathbf{x} - i\omega_n\tau} \phi_a(k)$. The action in momentum-Matsubara frequency space is

$$S_E = \int Dk \sum_a \phi_a^*(k) (\omega_n^2 + m_0^2) \phi_a(k) + \int \prod_{i=1}^4 Dk_i \sum_{ab} \phi_a^*(k_1)\phi_b^*(k_2)\phi_b(k_3)\phi_a(k_4)V(\{k_i\}), \quad (\text{A3})$$

where $k = (\mathbf{k}, \omega_n)$, $\int Dk = \frac{1}{\beta} \sum_n \int \frac{d^d k}{(2\pi)^d}$ and $V(\{k_i\}) = [\frac{\lambda_4}{N} + \frac{\lambda}{2N} \{|\mathbf{k}_1 - \mathbf{k}_2|^2 + |\mathbf{k}_3 - \mathbf{k}_4|^2\}] \delta(k_1 + k_2 - k_3 - k_4)$.

In the path integral we introduce an resolution of identity in terms of the correlator $G(k, k') = \sum_a \langle \phi_a^*(k) \phi_a(k') \rangle$ and a Lagrange multiplier $\Sigma(k, k')$ as $\mathbb{I} = \int DGD\Sigma e^{\int Dk Dk' \Sigma(k, k') [G(k, k') - \sum_a \langle \phi_a^*(k) \phi_a(k') \rangle]}$. With this the large- N action takes the form

$$S_N = \int Dk \sum_a \phi_a^*(k) [\omega_n^2 + \Sigma(k, k)] \phi_a(k) + m_0^2 \int Dk G(k, k) - \int Dk_1 Dk_2 \Sigma(k_1, k_2) G(k_1, k_2) + \int \prod_{i=1}^4 Dk_i G(k_1, k_3) G(k_2, k_4) V(\{k_i\}) \quad (\text{A4})$$

Integrating out $(N - 1)$ fields and setting $\sigma(k) = \langle \phi_{a=1}(k) \rangle / \sqrt{N}$, we get

$$S'_N = (N - 1) \int Dk \ln [\omega_n^2 + \Sigma(k, k)] + N \int Dk \sigma^*(k) (\omega_n^2 + \Sigma(k, k)) \sigma(k) + m_0^2 \int Dk G(k, k) - \int Dk_1 Dk_2 \Sigma(k_1, k_2) G(k_1, k_2) + \int \prod_{i=1}^4 Dk_i G(k_1, k_3) G(k_2, k_4) V(\{k_i\}). \quad (\text{A5})$$

By assuming translational invariance we have,

$$\begin{aligned} G(k, k') &= N\beta\delta_{n_1 n_2} (2\pi)^d \delta^d(\mathbf{k} - \mathbf{k}') G(k') \\ \Sigma(k, k') &= \beta\delta_{n_1 n_2} (2\pi)^d \delta^d(\mathbf{k} - \mathbf{k}') \Sigma(k') \text{ and} \\ \sigma(k) &= \beta\delta_{n_0} (2\pi)^d \delta^d(\mathbf{k}) \sigma, \end{aligned} \quad (\text{A6})$$

Putting all of these we get the effective action

$$S'_N = (N - 1) \int Dk \ln [\omega_n^2 + \Sigma(k)] + N\beta\delta_{n_0} (2\pi)^d \delta^d(\mathbf{k}) |\sigma|^2 \Sigma(k=0) + Nm_0^2 \int Dk G(k) - N \int Dk \Sigma(k) G(k) + N \int Dk Dk' NV(\mathbf{k}, \mathbf{k}'; \mathbf{k}, \mathbf{k}') G(k) G(k'). \quad (\text{A7})$$

Taking variation of the action with respect to Σ , G and σ we get the saddle point equations

$$\begin{aligned} G(k) &= \frac{1}{\omega_n^2 + \Sigma(k)} + \beta \delta_{n0} (2\pi)^d \delta^d(\mathbf{k}) |\sigma|^2 \\ \Sigma(k) &= m_0^2 + 2 \int Dk' NV(\mathbf{k}, \mathbf{k}'; \mathbf{k}, \mathbf{k}') G(k') \text{ and} \\ \sigma \Sigma(\mathbf{k} = 0) &= 0. \end{aligned} \quad (\text{A8})$$

It is clear that $\Sigma(k)$ only depends on the spatial component \mathbf{k} of the space-time vector $k = (\mathbf{k}, \omega_n)$ and it will represent square of the effective dispersion of the mode \mathbf{k} . So we set $\Sigma(k) = \omega(\mathbf{k})^2$. Final set of equations are given in Eq. 9. From Eq. 9a we can put the expression for $G(k)$ in Eq. 9b to get

$$\omega(\mathbf{k})^2 = m_0^2 + 2|\sigma|^2 NV(\mathbf{k}, 0; \mathbf{k}, 0) + 2 \int \frac{d^d k'}{(2\pi)^d} NV(\mathbf{k}, \mathbf{k}'; \mathbf{k}, \mathbf{k}') \frac{1}{\beta} \sum_n \frac{1}{\omega_n^2 + \omega(\mathbf{k}')^2} \quad (\text{A9})$$

Now the Matsubara sum becomes

$$\begin{aligned} \frac{1}{\beta} \sum_n \frac{1}{\omega_n^2 + \omega(\mathbf{k}')^2} &= -\frac{1}{\beta} \sum_n \frac{1}{(i\omega_n)^2 - \omega(\mathbf{k}')^2} \\ &= -\frac{1}{2\omega(\mathbf{k}')} \frac{1}{\beta} \sum_n \left[\frac{1}{i\omega_n - \omega(\mathbf{k}')} - \frac{1}{i\omega_n + \omega(\mathbf{k}')} \right] \\ &= \frac{1}{2\omega(\mathbf{k}')} [n_B(\omega(\mathbf{k}')) - n_B(-\omega(\mathbf{k}'))], \end{aligned} \quad (\text{A10})$$

where $n_B(\omega) = \frac{1}{e^{\beta\omega} - 1}$. So we get $\frac{1}{\beta} \sum_n \frac{1}{\omega_n^2 + \omega(\mathbf{k}')^2} = \frac{1}{2\omega(\mathbf{k}')} [1 + 2n_B(\omega(\mathbf{k}'))] = \frac{\coth\left(\frac{\omega(\mathbf{k}')}{2T}\right)}{2\omega(\mathbf{k}')}$. Putting this in Eq. A9, we get self-consistent equation for the dressed dispersion $\omega(\mathbf{k})$ (presented in Eq. 10 in the main text)

$$\omega(\mathbf{k})^2 = m_0^2 + 2|\sigma|^2 NV(\mathbf{k}, 0; \mathbf{k}, 0) + 2 \int \frac{d^d k'}{(2\pi)^d} NV(\mathbf{k}, \mathbf{k}'; \mathbf{k}, \mathbf{k}') \frac{\coth\left(\frac{\omega(\mathbf{k}')}{2T}\right)}{2\omega(\mathbf{k}')} \quad (\text{A11})$$

To regulate ultraviolet divergences we work on a lattice and use the regularized interaction (see Eq. 8) $NV_r(\mathbf{k}, \mathbf{k}'; \mathbf{k}, \mathbf{k}') = \lambda\epsilon(\mathbf{k} - \mathbf{k}') + \lambda_4$, where $\epsilon(\mathbf{k} - \mathbf{k}') = \frac{4}{a^2} \sum_{i=1}^d \sin^2\left(\frac{(k_i - k'_i)a}{2}\right)$ for a hyper cubic lattice in d dimension with lattice constant a . Using the structure of the interaction vertex, we can make the following ansatz for the dressed dispersion

$$\omega(\mathbf{k})^2 = m^2 + \kappa\epsilon(\mathbf{k}), \quad (\text{A12})$$

where m^2 is the gap and κ is related to the curvature or effective mass in kinetic sense. Putting this in Eq. 10 we get

$$m^2 + \kappa\epsilon(\mathbf{k}) = m_0^2 + 2|\sigma|^2 [\lambda_4 + \lambda\epsilon(\mathbf{k})] + 2 \int \frac{d^d k'}{(2\pi)^d} [\lambda_4 + \lambda\epsilon(\mathbf{k} - \mathbf{k}')] \frac{\coth\left(\frac{\omega(\mathbf{k}')}{2T}\right)}{2\omega(\mathbf{k}')} \quad (\text{A13})$$

Simplifying we get

$$m^2 + \kappa\epsilon(\mathbf{k}) = m_0^2 + 2|\sigma|^2 [\lambda_4 + \lambda\epsilon(\mathbf{k})] + 2 \int \frac{d^d k'}{(2\pi)^d} \left[\{\lambda_4 + \lambda\epsilon(\mathbf{k}')\} + \lambda \left\{ 1 - \frac{a^2}{2d} \epsilon(\mathbf{k}') \right\} \epsilon(\mathbf{k}) \right] \frac{\coth\left(\frac{\omega(\mathbf{k}')}{2T}\right)}{2\omega(\mathbf{k}')} \quad (\text{A14})$$

Equating co-efficient of $\epsilon(\mathbf{k})$ and \mathbf{k} -independent terms on both sides of Eq. A14 we get

$$m^2 = m_0^2 + 2|\sigma|^2 \lambda_4 + 2\lambda_4 I_1(m^2, \kappa) + 2\lambda I_2(m^2, \kappa) \text{ and} \quad (\text{A15a})$$

$$\kappa = 2|\sigma|^2 \lambda + 2\lambda [I_1(m^2, \kappa) - (a^2/2d) I_2(m^2, \kappa)], \quad (\text{A15b})$$

where $I_1(m^2, \kappa) = \int \frac{d^d k}{(2\pi)^d} \frac{\coth\left(\frac{\omega(\mathbf{k})}{2T}\right)}{2\omega(\mathbf{k})}$ and $I_2(m^2, \kappa) = \int \frac{d^d k}{(2\pi)^d} \frac{\epsilon(\mathbf{k}) \coth\left(\frac{\omega(\mathbf{k})}{2T}\right)}{2\omega(\mathbf{k})}$. We also have to satisfy $\sigma \Sigma(k) = \sigma \omega^2(\mathbf{k}) = 0$, which with our ansatz translates to $\sigma m^2 = 0$. This means either of σ and m^2 has to be zero. Setting $\sigma = 0$ we get the equations

for the normal phase depicted in Eq. 12 for $d = 3$. These equations represent a phase which conserve charge. The other set of equations can be found by setting $m^2 = 0$. These equations represent a condensed phase which breaks charge and consequently dipole symmetry and are presented in Eq. 13.

Appendix B: Phases and transition with varying coupling at $T=0$

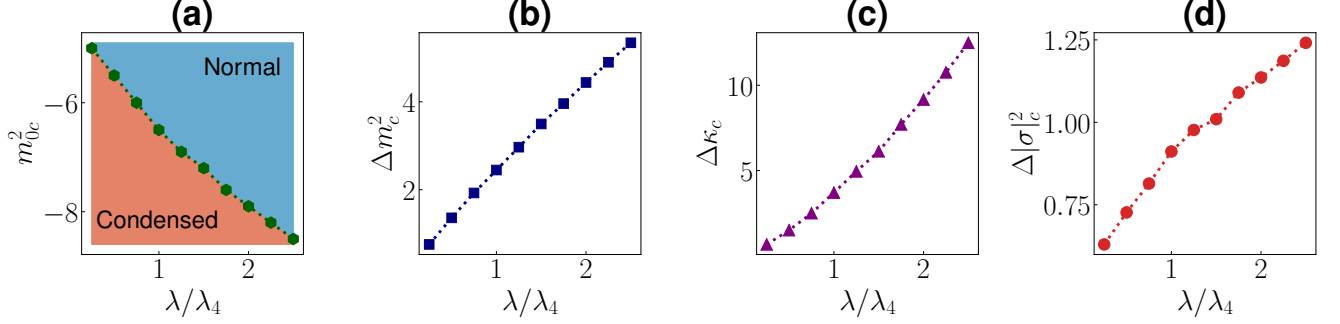


FIG. 7. Phases and transition at $T = 0$ for varying couplings. We keep $\lambda_4 = 2$ fixed and vary λ . (a) Critical m_{0c}^2 is plotted as a function of (λ/λ_4) . It decreases with (λ/λ_4) . The curve also represent the boundary between condensed phase (shaded in light red) and normal phase (shaded in light blue). (b)-(d) Jumps in the phase parameters at the transition are plotted with varying couplings. The jumps increases with (λ/λ_4) keeping the transition first-order in nature.

In this appendix we present more results about the phases and transition at equilibrium. In the main text we kept the couplings fixed at $\lambda_4 = 2$ and $\lambda = 2$ and we observed a discontinuous transition between a condensed phase ($U(N)$ and dipole symmetry broken) and a normal phase ($U(N)$ and dipole symmetry conserved). Here we investigate the phase diagram by changing λ while keeping $\lambda_4 = 2$ fixed. We find qualitatively similar behaviour here. In Fig. 7(a), we present the transition mass squared m_{0c}^2 as a function (λ/λ_4) . We see that m_{0c}^2 decreases as (λ/λ_4) is increased. This plot also represent the phase diagram in $(\lambda/\lambda_4) - m_0^2$ plane. The curve for m_{0c}^2 separates the two phases: condensed (shaded in light red) and normal (shaded in light blue). In Fig. 7(b)-(d), we plot the absolute value of the jumps in the phase parameters m^2 , κ and $|\sigma|^2$ respectively at the transition. The jumps increases with increasing (λ/λ_4) for all the parameters keeping the transition first-order in nature.

Appendix C: Phase parameters at thermal equilibrium

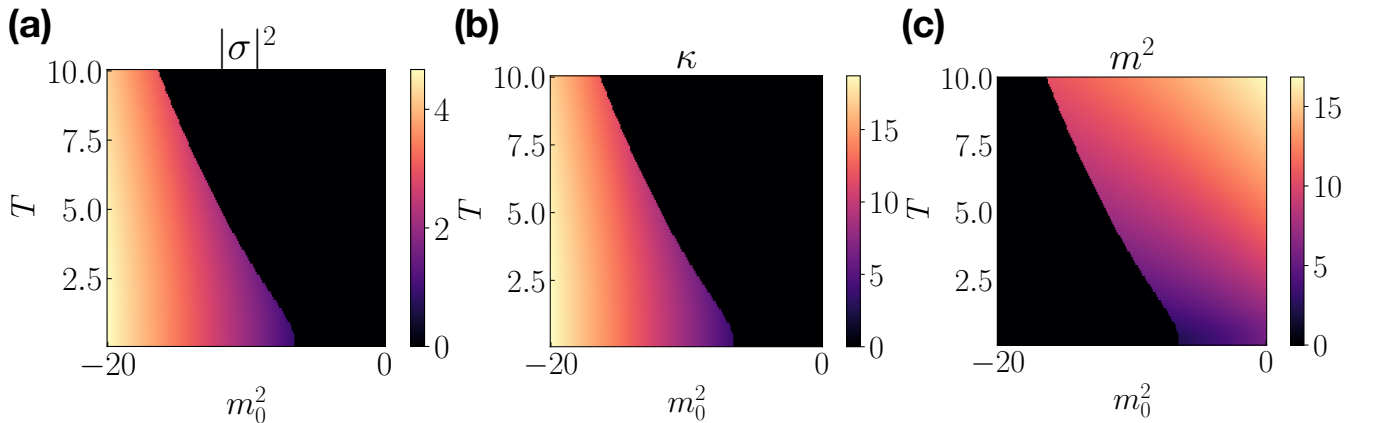


FIG. 8. Phase parameters of dipole conserving bosons at thermal equilibrium. (a), (b) and (c) Colormap of $|\sigma|^2$, κ and m^2 respectively on the $m_0^2 - T$ plane. The black regions represent 0 values. The coloured regions represent finite values given by the accompanying colorbars. The boundary between these two regions represent a first-order transition. $|\sigma|^2$ and κ are finite in the same region which hosts a condensed phase. On the other hand m^2 is finite in a region where $|\sigma|^2 = 0$ and $\kappa = 0$. This represents a normal phase. We also note that the phase parameters changes discontinuously at the transition which is the signature of the first order nature of the transition.

In this appendix we present the phase parameters at thermal equilibrium. Specifically we plot them as colormap on $m_0^2 - T$ to see their variation with the bare mass and temperature. Their values (finite or not) determines the phase. In Fig. 8 we present the colormaps of the phase parameters in $m_0^2 - T$ plane corresponding to the phase diagram presented in Fig. 2(e). In this figures, the black regions represent 0 values. The coloured regions represent finite values given by the accompanying colorbars. The boundary between these two regions represent a first-order transition. $|\sigma|^2$ and κ are finite in the same region which hosts a condensed phase. On the other hand m^2 is finite in a region where $|\sigma|^2 = 0$ and $\kappa = 0$. This represents a normal phase. We note that the phase parameters changes discontinuously at the transition which is the signature of the first order nature of the transition. We also note that the critical m_0^2 decreases with temperature.

Appendix D: Dynamical equations for parameters

In this appendix, we present the details of the method for the non-equilibrium dynamics of dipole conserving bosons. First, we derive the dynamical equations for the parameters in terms of one-body correlators. The correlators are evolved following SKFT for scalar field from Fock states⁶⁵ and described towards the end of this appendix. We initialize the system in the ground state of a particular phase with a fixed values of the phase parameters (m_{in}^2, κ_{in} and $|\sigma|_{in}^2$) corresponding to $m_0^2 = (m_0^2)_{in}$. The initial Keldysh correlator is related to these parameters as

$$iG^K(\mathbf{k}; t=0, t'=0) = \begin{cases} \frac{1}{2\sqrt{m_{in}^2 + \kappa_{in}\epsilon(\mathbf{k})}} & \text{for } \mathbf{k} \neq 0 \\ (2\pi)^d |\sigma|_{in}^2 & \text{for } \mathbf{k} = 0. \end{cases} \quad (\text{D1})$$

Now we proceed to describe how to calculate the phase parameters for the subsequent time in the case of time-dependent bare mass $m_0^2(t)$. Within the SKFT structure⁶⁴, the effective dispersion at any time is related to the retarded self-energy as

$$\omega^2(\mathbf{k}, t) = m_0^2(t) + \frac{1}{2}\Sigma^R(\mathbf{k}, t). \quad (\text{D2})$$

For the dynamics, the large- N (mean field) self-energy is given by the Hartree diagram⁶⁴. The retarded self-energy is given in terms of the interaction vertex and Keldysh correlator. To get the interaction vertex in Keldysh basis we write the interacting part of the action in terms of the fields in Keldysh basis as

$$\begin{aligned} S_{int} &= - \int \frac{d^d k}{(2\pi)^d} \int \frac{d^d k'}{(2\pi)^d} \int_0^\infty dt V_r(\mathbf{k}, \mathbf{k}'; \mathbf{k}, \mathbf{k}') [\phi_+^*(\mathbf{k}, t)\phi_+^*(\mathbf{k}', t)\phi_+(\mathbf{k}, t)\phi_+(\mathbf{k}', t) - \phi_-^*(\mathbf{k}, t)\phi_-^*(\mathbf{k}', t)\phi_-(\mathbf{k}, t)\phi_-(\mathbf{k}', t)] \\ &= - \int \frac{d^d k}{(2\pi)^d} \int \frac{d^d k'}{(2\pi)^d} \int_0^\infty dt V_K(\mathbf{k}, \mathbf{k}') [\phi_{cl}^*(\mathbf{k}, t)\phi_{cl}^*(\mathbf{k}', t)\phi_{cl}(\mathbf{k}, t)\phi_q(\mathbf{k}', t) + \phi_{cl}^*(\mathbf{k}, t)\phi_q^*(\mathbf{k}', t)\phi_{cl}(\mathbf{k}, t)\phi_{cl}(\mathbf{k}', t) \\ &\quad + \phi_q^*(\mathbf{k}, t)\phi_q^*(\mathbf{k}', t)\phi_q(\mathbf{k}, t)\phi_{cl}(\mathbf{k}', t) + \phi_q^*(\mathbf{k}, t)\phi_{cl}^*(\mathbf{k}', t)\phi_q(\mathbf{k}, t)\phi_q(\mathbf{k}', t)], \end{aligned} \quad (\text{D3})$$

where the vertex $V_K(\mathbf{k}, \mathbf{k}') = 4\lambda\epsilon(\mathbf{k} - \mathbf{k}') + 4\lambda_4 = 4V_r(\mathbf{k}, \mathbf{k}'; \mathbf{k}, \mathbf{k}')$. Going to the 2^{nd} line from the 1^{st} line, we have used the Keldysh rotated fields namely classical fields $\phi_{cl} = \frac{1}{2}(\phi_+ + \phi_-)$ and quantum fields $\phi_q = \frac{1}{2}(\phi_+ - \phi_-)$ ⁶⁴. Using this vertex we get the retarded self-energy

$$\Sigma^R(\mathbf{k}, t) = \int \frac{d^d k'}{(2\pi)^d} V_K(\mathbf{k}, \mathbf{k}') iG^K(\mathbf{k}'; t, t) + V_K(\mathbf{k}, 0)|\sigma|^2(t), \quad (\text{D4})$$

where $|\sigma|^2(t) = iG^K(\mathbf{k} = 0; t, t)/(2\pi)^d$. For the effective dispersion (Eq. D2) we get

$$\omega^2(\mathbf{k}, t) = m_0^2(t) + 2[\lambda_4 + \lambda\epsilon(\mathbf{k})]|\sigma|^2(t) + 2 \int \frac{d^d k'}{(2\pi)^d} \left[\{\lambda_4 + \lambda\epsilon(\mathbf{k}')\} + \lambda \left\{ 1 - \frac{a^2}{2d}\epsilon(\mathbf{k}') \right\} \epsilon(\mathbf{k}) \right] iG^K(\mathbf{k}'; t, t) \quad (\text{D5})$$

Using the parametrization $\omega^2(\mathbf{k}, t) = m^2(t) + \kappa(t)\epsilon(\mathbf{k})$ in analogy to the equilibrium case and comparing co-efficient of $\epsilon(\mathbf{k})$

and \mathbf{k} -independent terms in Eq. D5 we get

$$m^2(t) = m_0^2(t) + 2\lambda_4|\sigma|^2(t) + 2\lambda_4 \int \frac{d^d k}{(2\pi)^d} iG^K(\mathbf{k}; t, t) + 2\lambda \int \frac{d^d k}{(2\pi)^d} \epsilon(\mathbf{k}) iG^K(\mathbf{k}; t, t) \text{ and} \quad (\text{D6a})$$

$$\kappa(t) = 2\lambda|\sigma|^2(t) + 2\lambda \int \frac{d^d k}{(2\pi)^d} iG^K(\mathbf{k}; t, t) - 2\lambda(a^2/2d) \int \frac{d^d k}{(2\pi)^d} \epsilon(\mathbf{k}) iG^K(\mathbf{k}; t, t). \quad (\text{D6b})$$

Now we describe the time-evolutions of one-body correlators. Dynamics of the correlators are required to get the time-evolution of the parameters. We are concerned about the dynamics of the one-body correlators of the SKFT structure, namely the retarded correlator $iG^R(\mathbf{k}; t, t') = \langle \phi_{cl}(\mathbf{k}, t) \phi_q^*(\mathbf{k}, t') \rangle$ and Keldysh correlator $iG^K(\mathbf{k}; t, t') = \langle \phi_{cl}(\mathbf{k}, t) \phi_{cl}^*(\mathbf{k}, t') \rangle$. Within the mean field approximation, there is only Hartree diagram for retarded self-energy and there is no Keldysh self-energy. If we start from a Fock state with mode energies $\omega_{in}(\mathbf{k})$, the correlators are determined by

$$2[-\partial_t^2 - m^2(t) - \kappa(t)\epsilon(\mathbf{k})] G^R(\mathbf{k}, t, t') = \delta(t - t') \text{ and} \quad (\text{D7a})$$

$$G^K(\mathbf{k}; t, t) = [2\omega_{in}(\mathbf{k})]^2 G^K(\mathbf{k}; 0, 0) \left\{ |G^R(\mathbf{k}; t, 0)|^2 + \frac{1}{[\omega_{in}(\mathbf{k})]^2} |\bar{G}^R(\mathbf{k}; t, 0)|^2 \right\}, \quad (\text{D7b})$$

where $\bar{G}^R(\mathbf{k}; t, t') = \partial_{t'} G^R(\mathbf{k}; t, t')$. So, we now have closed set of equations for the dynamics of the parameters $m^2(t)$, $\kappa(t)$ and $|\sigma|^2(t)$ and the correlators $G^R(\mathbf{k}; t, t')$ and $G^K(\mathbf{k}; t, t)$.

* mursalin@theory.tifr.res.in

- ¹ M. Pretko, *Phys. Rev. B* **98**, 115134 (2018).
- ² K. Jensen and A. Raz, “Large n fractons,” (2022), [arXiv:2205.01132 \[hep-th\]](https://arxiv.org/abs/2205.01132).
- ³ A. Jain, K. Jensen, R. Liu, and E. Mefford, (2023), [arXiv:2304.09852 \[hep-th\]](https://arxiv.org/abs/2304.09852).
- ⁴ J. Armas and E. Have, “Ideal fracton superfluids,” (2023), [arXiv:2304.09596 \[hep-th\]](https://arxiv.org/abs/2304.09596).
- ⁵ P. Gorantla, H. T. Lam, N. Seiberg, and S.-H. Shao, *Phys. Rev. B* **106**, 045112 (2022).
- ⁶ S. Han, A. S. Patri, and Y. B. Kim, *Phys. Rev. B* **105**, 235120 (2022).
- ⁷ R. M. Nandkishore, W. Choi, and Y. B. Kim, *Phys. Rev. Res.* **3**, 013254 (2021).
- ⁸ E. Lake, M. Hermele, and T. Senthil, *Phys. Rev. B* **106**, 064511 (2022).
- ⁹ A. G. Burchards, J. Feldmeier, A. Schuckert, and M. Knap, *Phys. Rev. B* **105**, 205127 (2022).
- ¹⁰ P. Zechmann, E. Altman, M. Knap, and J. Feldmeier, *Phys. Rev. B* **107**, 195131 (2023).
- ¹¹ E. Lake, H.-Y. Lee, J. H. Han, and T. Senthil, *Phys. Rev. B* **107**, 195132 (2023).
- ¹² P. Gorantla, H. T. Lam, N. Seiberg, and S.-H. Shao, *Phys. Rev. B* **104**, 235116 (2021).
- ¹³ N. Seiberg and S.-H. Shao, *SciPost Phys.* **9**, 046 (2020).
- ¹⁴ N. Seiberg and S.-H. Shao, *SciPost Phys.* **10**, 027 (2021).
- ¹⁵ W. Shirley, K. Slagle, Z. Wang, and X. Chen, *Phys. Rev. X* **8**, 031051 (2018).
- ¹⁶ K. Slagle, *Phys. Rev. Lett.* **126**, 101603 (2021).
- ¹⁷ K. Slagle and Y. B. Kim, *Phys. Rev. B* **97**, 165106 (2018).
- ¹⁸ M. Pretko, *Phys. Rev. B* **95**, 115139 (2017).
- ¹⁹ J. Haah, *Phys. Rev. A* **83**, 042330 (2011).
- ²⁰ S. Vijay, J. Haah, and L. Fu, *Phys. Rev. B* **94**, 235157 (2016).
- ²¹ N. Seiberg, *SciPost Phys.* **8**, 050 (2020).
- ²² R. M. Nandkishore and M. Hermele, *Annual Review of Condensed Matter Physics* **10**, 295 (2019).
- ²³ M. Pretko, X. Chen, and Y. You, *International Journal of Modern Physics A* **35**, 2030003 (2020).
- ²⁴ T. N. Ikeda and M. Sato, *Science Advances* **6**, eabb4019 (2020).
- ²⁵ M. H. Szymańska, J. Keeling, and P. B. Littlewood, *Phys. Rev. Lett.* **96**, 230602 (2006).
- ²⁶ B. Buča, J. Tindall, and D. Jaksch, *Nature Communications* **10**, 1730 (2019).
- ²⁷ J. Eisert, M. Friesdorf, and C. Gogolin, *Nature Physics* **11**, 124 (2015).
- ²⁸ J. Bloch, I. Carusotto, and M. Wouters, *Nature Reviews Physics* **4**, 470 (2022).
- ²⁹ E. A. Goldschmidt, T. Boulier, R. C. Brown, S. B. Koller, J. T. Young, A. V. Gorshkov, S. L. Rolston, and J. V. Porto, *Phys. Rev. Lett.* **116**, 113001 (2016).
- ³⁰ J. F. Poyatos, J. I. Cirac, and P. Zoller, *Phys. Rev. Lett.* **77**, 4728 (1996).
- ³¹ S. Diehl, A. Micheli, A. Kantian, B. Kraus, H. P. Büchler, and P. Zoller, *Nature Physics* **4**, 878 (2008).
- ³² M. Müller, S. Diehl, G. Pupillo, and P. Zoller, in *Advances in Atomic, Molecular, and Optical Physics*, Advances In Atomic, Molecular, and Optical Physics, Vol. 61, edited by P. Berman, E. Arimondo, and C. Lin (Academic Press, 2012) pp. 1–80.
- ³³ H. P. Lüschen, P. Bordia, S. S. Hodgman, M. Schreiber, S. Sarkar, A. J. Daley, M. H. Fischer, E. Altman, I. Bloch, and U. Schneider, *Phys. Rev. X* **7**, 011034 (2017).
- ³⁴ F. Verstraete, M. M. Wolf, and J. Ignacio Cirac, *Nature Physics* **5**, 633 (2009).
- ³⁵ C. N. Yang, *Phys. Rev. Lett.* **63**, 2144 (1989).
- ³⁶ S. Moudgalya, N. Regnault, and B. A. Bernevig, *Phys. Rev. B* **102**, 085140 (2020).
- ³⁷ E. Demler and S.-C. Zhang, *AIP Conference Proceedings* **483**, 30 (1999).
- ³⁸ J. M. Deutsch, *Phys. Rev. A* **43**, 2046 (1991).
- ³⁹ M. Srednicki, *Phys. Rev. E* **50**, 888 (1994).
- ⁴⁰ M. Srednicki, *Journal of Physics A: Mathematical and General* **32**, 1163 (1999).

- ⁴¹ M. Rigol, V. Dunjko, and M. Olshanii, *Nature* **452**, 854 (2008).
- ⁴² P. Reimann, *Phys. Rev. Lett.* **101**, 190403 (2008).
- ⁴³ A. C. Cassidy, C. W. Clark, and M. Rigol, *Phys. Rev. Lett.* **106**, 140405 (2011).
- ⁴⁴ P. Banerjee, A. Gaikwad, A. Kaushal, and G. Mandal, *Journal of High Energy Physics* **2020**, 27 (2020).
- ⁴⁵ Q.-Q. Wang, S.-J. Tao, W.-W. Pan, Z. Chen, G. Chen, K. Sun, J.-S. Xu, X.-Y. Xu, Y.-J. Han, C.-F. Li, and G.-C. Guo, *Light: Science & Applications* **11**, 194 (2022).
- ⁴⁶ D. Basko, I. Aleiner, and B. Altshuler, *Annals of Physics* **321**, 1126 (2006).
- ⁴⁷ M. Schreiber, S. S. Hodgman, P. Bordia, H. P. Lüschen, M. H. Fischer, R. Vosk, E. Altman, U. Schneider, and I. Bloch, *Science* **349**, 842 (2015).
- ⁴⁸ J. yoon Choi, S. Hild, J. Zeiher, P. Schauß, A. Rubio-Abadal, T. Yefsah, V. Khemani, D. A. Huse, I. Bloch, and C. Gross, *Science* **352**, 1547 (2016).
- ⁴⁹ R. Nandkishore and D. A. Huse, *Annual Review of Condensed Matter Physics* **6**, 15 (2015).
- ⁵⁰ F. Alet and N. Laflorencie, *Comptes Rendus Physique* **19**, 498 (2018).
- ⁵¹ D. A. Abanin, E. Altman, I. Bloch, and M. Serbyn, *Rev. Mod. Phys.* **91**, 021001 (2019).
- ⁵² A. Chakraborty, P. Gorantla, and R. Sensarma, *Phys. Rev. B* **102**, 224306 (2020).
- ⁵³ J. Berges, S. Borsányi, and C. Wetterich, *Phys. Rev. Lett.* **93**, 142002 (2004).
- ⁵⁴ T. Kinoshita, T. Wenger, and D. S. Weiss, *Nature* **440**, 900 (2006).
- ⁵⁵ M. Gring, M. Kuhnert, T. Langen, T. Kitagawa, B. Rauer, M. Schreitl, I. Mazets, D. A. Smith, E. Demler, and J. Schmiedmayer, *Science* **337**, 1318 (2012).
- ⁵⁶ K. Mallayya, M. Rigol, and W. De Roeck, *Phys. Rev. X* **9**, 021027 (2019).
- ⁵⁷ A. Kyprianidis, F. Machado, W. Morong, P. Becker, K. S. Collins, D. V. Else, L. Feng, P. W. Hess, C. Nayak, G. Pagano, N. Y. Yao, and C. Monroe, *Science* **372**, 1192 (2021).
- ⁵⁸ D. V. Else, B. Bauer, and C. Nayak, *Phys. Rev. X* **7**, 011026 (2017).
- ⁵⁹ M. Serbyn, D. A. Abanin, and Z. Papic, *Nature Physics* **17**, 675 (2021).
- ⁶⁰ B. Mukherjee, S. Nandy, A. Sen, D. Sen, and K. Sengupta, *Phys. Rev. B* **101**, 245107 (2020).
- ⁶¹ B. Mukherjee, A. Sen, D. Sen, and K. Sengupta, *Phys. Rev. B* **102**, 075123 (2020).
- ⁶² S. Ghosh, I. Paul, and K. Sengupta, *Phys. Rev. Lett.* **130**, 120401 (2023).
- ⁶³ J. Marino, M. Eckstein, M. S. Foster, and A. M. Rey, *Reports on Progress in Physics* **85**, 116001 (2022).
- ⁶⁴ A. Kamenev, *Field Theory of Non-Equilibrium Systems* (Cambridge University Press, New York, 2011).
- ⁶⁵ M. M. Islam and R. Sensarma, *Phys. Rev. B* **106**, 024306 (2022).
- ⁶⁶ A. Kamenev and A. Levchenko, *Advances in Physics* **58**, 197 (2009).
- ⁶⁷ A. Chakraborty, P. Gorantla, and R. Sensarma, *Phys. Rev. B* **99**, 054306 (2019).
- ⁶⁸ A. Chakraborty and R. Sensarma, *Phys. Rev. B* **97**, 104306 (2018).
- ⁶⁹ L. M. Sieberer, M. Buchhold, and S. Diehl, *Reports on Progress in Physics* **79**, 096001 (2016).
- ⁷⁰ S. R. Das and K. Sengupta, *Journal of High Energy Physics* **2012**, 72 (2012).
- ⁷¹ A. Chandran and S. L. Sondhi, *Phys. Rev. B* **93**, 174305 (2016).
- ⁷² A. Chandran, A. Nanduri, S. S. Gubser, and S. L. Sondhi, *Phys. Rev. B* **88**, 024306 (2013).
- ⁷³ A. Larzul and M. Schiró, *Phys. Rev. B* **105**, 045105 (2022).
- ⁷⁴ S. Sankar and V. Tripathi, *Phys. Rev. B* **99**, 245113 (2019).
- ⁷⁵ I. Jang and P.-Y. Chang, “Thermalization and transient dynamics in multi-channel kondo systems under the quantum quench: Large- n schwinger-keldysh approach,” (2023), [arXiv:2303.02433 \[cond-mat.str-el\]](https://arxiv.org/abs/2303.02433).
- ⁷⁶ D. Das and B. Dey, *Journal of High Energy Physics* **2020**, 107 (2020).